Check for updates

The lateral superior olive in the mouse: Two systems of projecting neurons

Isabella R. Williams [1,2]*, Anastasia Filimontseva [1],
Catherine J. Connelly [1,2]† and David K. Ryugo [1,2,3]

[1]Garvan Institute of Medical Research, Darlinghurst, NSW, Australia, [2]School of Medical Sciences,
University of New South Wales, Kensington, NSW, Australia, [3]Department of Otolaryngology-Head,
Neck and Skull Base Surgery, St. Vincent's Hospital, Darlinghurst, NSW, Australia

The lateral superior olive (LSO) is a key structure in the central auditory system of mammals that exerts efferent control on cochlear sensitivity and is involved in the processing of binaural level differences for sound localization. Understanding how the LSO contributes to these processes requires knowledge about the resident cells and their connections with other auditory structures. We used standard histological stains and retrograde tracer injections into the inferior colliculus (IC) and cochlea in order to characterize two basic groups of neurons: (1) Principal and periolivary (PO) neurons have projections to the IC as part of the ascending auditory pathway; and (2) lateral olivocochlear (LOC) intrinsic and shell efferents have descending projections to the cochlea. Principal and intrinsic neurons are intermixed within the LSO, exhibit fusiform somata, and have disk-shaped dendritic arborizations. The principal neurons have bilateral, symmetric, and tonotopic projections to the IC. The intrinsic efferents have strictly ipsilateral projections, known to be tonotopic from previous publications. PO and shell neurons represent much smaller populations (<10% of principal and intrinsic neurons, respectively), have multipolar somata, reside outside the LSO, and have non-topographic, bilateral projections. PO and shell neurons appear to have widespread projections to their targets that imply a more diffuse modulatory function. The somata and dendrites of principal and intrinsic neurons form a laminar matrix within the LSO and share quantifiably similar alignment to the tonotopic axis. Their restricted projections emphasize the importance of frequency in binaural processing and efferent control for auditory perception. This study addressed and expanded on previous findings of cell types, circuit laterality, and projection tonotopy in the LSO of the mouse.

KEYWORDS

anatomy, auditory, isofrequency, lateral superior olive, olivocochlear efferents, tonotopy, topography

Introduction

The perception of auditory space is initiated by the complementary actions of multiple auditory brainstem nuclei. Anatomical and physiological data implicate the medial superior olive in the processing of interaural time differences, the lateral superior olive (LSO) and medial nucleus of the trapezoid body (MNTB) in decoding interaural level differences, and the dorsal cochlear nucleus (CN) for analyzing spectral cues created by head and pinna reflections (Young et al., 1992; Joris, 1996; Joris and Yin, 1998; Konishi et al., 2003; Reiss and Young, 2005; Middlebrooks, 2015; Franken et al., 2018; Joris and van der Heijden, 2019). The LSO is part of the superior olivary complex (SOC), located at the base of the pontine-medullary junction and is one of the earliest structures to receive binaural inputs. Basic knowledge about LSO cell morphology and how they are synaptically connected represents an important first step to understanding the circuits for the localization and separation of sounds.

Auditory information that reaches the LSO originates directly from ipsilateral spherical bushy and planar multipolar cells of the anteroventral cochlear nucleus (AVCN; Cant and Casseday, 1986; Doucet and Ryugo, 2003) and indirectly from contralateral globular bushy cells of the AVCN by way of the MNTB (Warr, 1966; Tolbert et al., 1982; Glendenning et al., 1985; Banks and Smith, 1992; Henkel and Gabriele, 1999). The convergence of these two inputs, one excitatory and the other inhibitory, are matched in frequency tuning and temporal characteristics for analysis of interaural level differences, a primary cue for localizing high frequency sounds (Yin et al., 2019). The result of this binaural processing is sent along ascending pathways for further encoding of spatial location (Tollin, 2003; Middlebrooks and Waters, 2020) and down descending pathways to modulate cochlear sensitivity in ways yet to be fully understood.

The LSO contains a heterogeneous population of neurons that have been categorized on the basis of somatic size, dendritic morphology, location (Ollo and Schwartz, 1979; Cant, 1984; Helfert and Schwartz, 1986, 1987; Rietzel and Friauf, 1998; Kulesza, 2008), chemical markers (Helfert et al., 1989; Eybalin, 1993), or projections (Adams, 1979; Glendenning and Masterton, 1983; Henkel and Brunso-Bechtold, 1993). These different neuron groups are presumably involved in separate aspects of processing and dispensing this information. The

---

Abbreviations: AChE, acetylcholinesterase; AR, antonia red dextran 4; AVCN, anteroventral cochlear nucleus; C, caudal; CF, characteristic frequency; ChAT, choline acetyltransferase; CN, cochlear nucleus; CNIC, central nucleus of the inferior colliculus; CTB, cholera toxin subunit–B; CV, cresyl violet; D, dorsal; DH, dorsal hilus; DAB, 3,3′-diaminobenzene; FD, fluorescein dextran; FG, fluorogold; IC, inferior colliculus; L, lateral; LOC, lateral olivocochlear; LSO, lateral superior olive; MNTB, medial nucleus of the trapezoid body; MOC, medial olivocochlear; NiDAB, nickel intensified DAB; OC, olivocochlear; PO, periolivary; SOC, superior olivary complex.

dominant LSO cell type is the principal neuron and they have ascending projections up the midbrain (Adams, 1979; Glendenning and Masterton, 1983; Cant, 1984; Helfert and Schwartz, 1986). Other cell types have been described and vary with respect to species, staining technique, taxonomic criteria, and observer. Four cell types are proposed for the cat (Helfert and Schwartz, 1986), four for the gerbil (Helfert and Schwartz, 1987), three for the mouse (Ollo and Schwartz, 1979), three for the human (Kulesza, 2007), and seven for the rat (Rietzel and Friauf, 1998). The main limitation to these taxonomic schemes is that they do not include circuit information and they are founded on observations collected from different species of widely different ages, crucial variables known to influence structure and function (Ryugo and Fekete, 1982; Romand, 1983; Brugge, 1988; Jenkins and Simmons, 2006; Van Hooser, 2007).

The other main type of LSO neuron in the mouse is the intrinsic neuron, which comprises the group of lateral olivocochlear (LOC) efferents, whose axonal projections terminate under inner hair cells of the cochlea primarily against the peripheral processes of auditory nerve fibers (Warr and Guinan, 1979). Intrinsic neurons are intermixed with the principal cells in rodents (White and Warr, 1983; Aschoff and Ostwald, 1987; Campbell and Henson, 1988; Vetter and Mugnaini, 1992; Yao and Godfrey, 1995; Safieddine et al., 1997; Sánchez-González et al., 2003; Mulders and Robertson, 2004; Brown, 2011; Romero and Trussell, 2021). In other mammals, such as cats, squirrel monkeys, and humans, members of the LOC system may be found outside the LSO in various periolivary nuclei (Warr, 1975; Thompson and Thompson, 1986; Aschoff and Ostwald, 1987; Bishop and Henson, 1987; Brown et al., 1988; Moore, 2000). The functional significance of the location of these efferent cell bodies is unknown.

The principal neuron is the dominant cell type in the LSO but there are disagreements with respect to the laterality of their ascending projections. They have been qualitatively reported as bilateral and symmetric (Adams, 1979; Schweizer, 1981; Nordeen et al., 1983; Ross et al., 1988; Grothe, 1994; Kelly et al., 1998) or with a contralateral preference (Brunso-Bechtold et al., 1981; Willard and Martin, 1984; Moore et al., 1995; Mellott et al., 2021). There are reports that (1) ipsilateral projections are glycinergic and entirely inhibitory (Saint Marie et al., 1989; Saint Marie and Baker, 1990), (2) ipsilateral projections are primarily low frequency, whereas high frequency projections are mostly contralateral (cats, Glendenning and Masterton, 1983; Oliver, 2000); and (3) low frequencies project contralaterally, whereas high frequencies project ipsilaterally (ferrets, Henkel and Brunso-Bechtold, 1993).

A tonotopic organization has been shown for the LSO (Boudreau and Tsuchitani, 1970; Guinan et al., 1972; Sanes and Rubel, 1988; Sanes et al., 1990) and IC (Rose et al., 1963; Merzenich and Reid, 1974; FitzPatrick, 1975; Stiebler and Ehret, 1985). This organization for the LSO appears dependent on its topographic and tonotopic input from the CN as well as

from the MNTB (Friauf and Ostwald, 1988; Sommer et al., 1993; Doucet and Ryugo, 2003; Gómez-Álvarez and Saldaña, 2015). The IC gets tonotopic input from the CN (Ross et al., 1988; Oliver et al., 1997; Malmierca et al., 2005). Topographic and tonotopic connections between the IC and LSO have been reported using large injections of a retrograde tracer in cats (Brunso-Bechtold et al., 1981) and rats (Kelly et al., 1998) but a more detailed analysis of this pathway is merited.

The data on the LSO have been collected under a variety of different conditions, perhaps accounting for some of the disagreements in the literature. The aims of this study in the adult mouse were (1) to address the cell types of the LSO; (2) to determine quantitatively if the projection of principal neurons to the IC is symmetric; and (3) to expand on previous findings of LSO topography and tonotopy.

Materials and methods

Mouse model of hearing

This study was performed in strict accordance with the Australian Code for the Care and Use of Animals for Scientific Purposes (2013). All of the animals were handled according to Animal Ethics Committee protocols (Animal Research Authority: 19-33, 20-02, and 21-13) approved by the Garvan/St Vincent's Hospital Animal Ethics Committee. All procedures were conducted under appropriate anesthesia and analgesia with animal welfare consideration underpinned by the principles of Replacement, Reduction and Refinement. A total of 44 healthy CBA/CaH mice of either sex and between the ages of 3–8 months were used.

Hearing status

All animals underwent auditory brainstem response testing prior to experimentation. Animals were positioned in a double-walled, sound-attenuating chamber (Sonora Technology, Gotenba, Japan) on a heating pad under ketamine/xylazine (100 mg/kg; 20 mg/kg) anesthesia. When areflexic to a toe-pinch, the recording, reference, and ground electrodes were positioned beneath the skin above the vertex, left pinna, and biceps femoris, respectively. A speaker was positioned 45° off the midline and 10 cm from the pinna where alternating condensation and rarefaction click stimuli (100 μsec square wave pulses) and tone stimuli at 4, 8, 16, 24, 32, 40, and 48 kHz (5 ms duration, 0.5 ms rise/fall) were generated using a software-controlled signal processor [RZ6/BioSigRZ; Tucker-Davis Technologies (TDT)] and delivered from 90 to 30 dB SPL in 10 dB decremental steps to either ear separately. Stimulus presentations (n = 512)

were delivered at a rate of 10/s for each level and the evoked responses were amplified (RA16PA/RA4LI; TDT), bandpass filtered from 0.5 to 3 kHz, recorded, and averaged (RZ6; TDT). Only mice with normal auditory brainstem response thresholds and audiograms (Zheng et al., 1999; Taberner and Liberman, 2005; Muniak et al., 2018) were used in this study.

Neuronal tract tracing

Inferior colliculus injections

Injections of retrograde tracers, Fluorescein Dextran (FD-3000MW, biotinylated, 5% in saline; Cat #D3305, Invitrogen/Molecular Probes, Scoresby, VIC, Australia), Fluorogold (FG; 4% in saline, Fluorochrome, Denver, CO, USA), Cholera Toxin Subunit-B (CTB; 0.5% in saline; List Biological Laboratories, Campbell, CA, USA) and Antonia Red Dextran 4 (AR; 10% saline; cat# 79672, Sigma Aldrich, St Louis, MO, USA) were made iontophoretically (**Supplementary material 1**) or *via* pressure (up to 0.5 μL) into the central nucleus of the IC. Pressure injections were used in the IC to maximize the labeling of the principal neurons in the LSO, particularly to show their neuronal distribution within the nucleus.

The IC surgical approach began by making a skin incision on the dorsal surface of the head to expose the cranial sutures, bregma and lambda. Approximately 5.2 mm posterior to bregma, a craniotomy (roughly 2 mm^2) was made overlying the IC. A glass micropipette (20–60 μm, inside tip diameter) was positioned on a micromanipulator and used to pressure inject 0.5 μL of tracer (100 nL/min) into the IC at a depth of 1.0–1.5 mm (stereotaxic coordinates of Paxinos and Franklin, 2008). Bilateral injections into each IC were performed with FD and FG to visualize the bilateral projection property of both IC (as above, n = 7). Following IC injections, bone wax was applied to cover the craniotomy, and VetBond tissue adhesive was used to close the incision site for the post-surgical survival period. Retrograde tracers were placed in both the IC and cochlea of a mouse (n = 4) in order to label LSO neurons with ascending and descending projections in the same LSO.

Cochlea injections

The surgical approach to the cochlea involved a post-auricular incision and removal of the tympanic membrane and the ossicular chain. With the middle ear opened, a microliter syringe was used to inject 0.5–1 μL of tracer directly into the round window (n = 21). After injection, the round window was plugged with bone-wax to prevent tracer leakage, bupivacaine (0.05 mL) was injected subcutaneously at the incision site, and VetBond was used to close the incision. The animal survived 14 days following the injection.

Tissue processing

Animals were euthanized with an intraperitoneal injection of Lethabarb (0.1 mg/kg) and perfused transcardially with 3–5 mL of 1% sodium nitrate in phosphate-buffered saline, followed by 60 mL of 4% paraformaldehyde (0.1M phosphate buffer, pH 7.4). The head was removed, the calvaria partially opened to expose the brain, and the head post-fixed for two-three hours. The brain was then completely dissected out of the skull and post-fixed overnight at room temperature in 0.1M buffered 4% paraformaldehyde. The next day, the brain was embedded in a gelatin-albumin mixture hardened with 4% paraformaldehyde and sectioned into 60 μm-thick sections using a vibrating microtome (Leica VT1200S, Nussloch, DE).

Cresyl violet (CV) staining was routinely performed on sections mounted on slides using a protocol modified from Humason (1979). The sections were hydrated in distilled water for 5 min, followed by a 10-min incubation in 0.1% CV dye at room temperature. The slides were rinsed in distilled water, followed by rinses in 70% alcohol, 95% alcohol and then differentiated (95% alcohol with 10 drops of glacial acetic acid) for one minute to remove excess staining. Rehydration in decreasing concentration of alcohol (one-minute periods in 70, 50, 30%, and distilled water) further removes excess CV for air-drying overnight and cover slipping with Permount the next day.

Cholinergic staining

Cholinergic markers, choline acetyltransferase (ChAT; $n = 7$) or acetylcholinesterase (AChE; $n = 3$), were used to visualize the cholinergic neurons of the LSO. The two methods were used to confirm cell counts and size measurements. Immunohistochemical processing of ChAT was performed on free-floating sections. Sections were washed 3x for 5 min each in 0.12M-Tris buffered saline, placed in 3% hydrogen peroxide for 10 min, followed by washes with Tris buffered saline, incubated in 0.1% Photoflo (Kodak, Rochester, NY, USA) for 1 h, and followed by an hour in 10% normal goat serum. Sections were washed and incubated at 4°C overnight in 1:1000 mouse anti-ChAT primary antibody (Cat #VP- C3838; RRID:AB_2336337; Vector Labs, Newark, CA, USA) and 2% normal goat serum. Negative control sections were unexposed to primary antibody. The following day, sections were rinsed and incubated for one hour in 1:200 biotinylated goat anti-mouse secondary antibody (Cat #BA-9200, Vector Labs, Burlingame, CA, USA). Sections were rinsed and then developed in a solution of 0.005% 3,3'-diaminobenzene (DAB) with 0.03% hydrogen peroxide until a distinct brown reaction product appeared in the tissue or intensified by the addition of nickel ammonium sulfate to produce a deep purple reaction product (NiDAB).

All sections were mounted and coverslipped with Permount (ThermoFisher, Waltham, MA, USA) for examination by brightfield microscopy.

Cholinergic staining for AChE was performed on glass-mounted tissue sections using a standard protocol (Karnovsky and Roots, 1964). Briefly, the slides were incubated in acetylcholine medium for 30 minutes, followed by 6 × 30 s rinses in distilled water, then incubated in 4% sodium sulfide solution for 1 min, followed by 2 × 30 s rinses in distilled water. The tissue was "toned" in 1% silver nitrate for 30 s, rinsed 6 × 30 s in distilled water, air dried overnight, and then coverslipped with Permount. LOC cell counts and measurements confirmed labeling equality for ChAT and AChE.

Fluorescent tracer processing

All cases with fluorescent tracer injections were visualized with standard fluorescent microscopy. The tissue sections were cut, mounted immediately, and coverslipped with VectaShield (H-1400; Vector Labs, Newark, CA, USA). In cases where chromogenic processing was performed after fluorescent imaging, the coverslips were removed, and the tissue was processed accordingly.

Immunohistochemical processing of neuronal tracers

Thirteen injection cases with tracer deposits of FG, FD, and/or CTB were processed by chromogenic development. Free-floating tissue sections were placed in serial order in 24-well plates. Sections were washed in 0.12M Tris buffered saline, treated with 3% hydrogen peroxide for 10 min, rinsed, and permeabilized in 0.1% Photoflo (Kodak, Rochester, NY, USA) for one hour. Tissue processed for biotinylated FD were then incubated for one hour in avidin-biotin complex (Vectastain Elite ABC Kit, Cat# PK-6100; Vector Labs, Newark, CA, USA) before undergoing development with DAB (as above).

Tissue processed for FG were incubated for one hour in 10% normal goat serum (Cat#VES100020, Vector Labs, Newark, CA, USA), whereas CTB-tissue was placed in 1% normal rabbit serum (Cat # S-5000; Vector Laboratories, Burlingame, CA, USA). The tissue then underwent 3x rinses for 5 min, before being placed at 4°C overnight in 1:100 rabbit anti-FG primary antibody and 2% normal rabbit serum (Cat#R4880, Sigma Aldrich, St Louis, MO, USA) or polyclonal goat anti-CTB primary antibody (1:10,000; Cat# 703, RRID:AB_10013220; List Biological Laboratories) with 2% normal goat serum. Negative control sections were not exposed to primary antibody. FG sections were rinsed and incubated in biotinylated goat anti-rabbit secondary (Cat #AB207995, Abcam, Cambridge, United Kingdom) and CTB sections were incubated in

biotinylated rabbit anti-goat secondary (1:200; Cat# BA-5000; Vector Labs) for one hour, rinsed, and incubated for one hour in avidin-biotin complex. Sections were developed with either 0.005% 3,3'-diaminobenzene (DAB) or nickel-intensified DAB (NiDAB). Some cases were counterstained with CV. In cases where two tracers were injected, FD was processed prior to FG. All sections were mounted and coverslipped with Permount for examination with brightfield microscopy.

Quantification of the lateral superior olive neuronal cohorts and statistics

Photomontages of serial sections were created from low magnifications (2.5x, 10x, and 20x objectives) from the facial nucleus to the ventral nucleus of the lateral lemniscus to identify the boundary of the LSO. Cell measurements of the different neuron types was made from high magnification brightfield and fluorescent micrographs (40x Plan-Apochromat or 100x Neofluar objectives). Micrographs of the LSO was created by making z-stacks from 4 to 5 focal planes using *Photoshop* software (300 dpi resolution) (Adobe Photoshop, 2021), and the micrographs were pieced together into montages to cover the entire LSO. Only cells with a visible nucleus were included for analysis. The size of principal and intrinsic neurons were compared in male and female mice aged from 3 to 8 months and the sizes of principal cells, POs, intrinsic cells, and shell neurons were all compared with respect to the different staining methods. There is no statistical size difference created by age, sex, or staining methods for the data reported (**Supplementary material 2** and **Supplementary Tables 1–3**). Positive controls for our cell size method were provided by results calculated from vesicular Glutamate Transporter-2-stained principal cells and AChE-stained intrinsic cells of the Allen Brain Atlas (Brain Map - brain-map.org, 2021). There was no difference when comparing average somatic areas from our tissue to these other two data sets (vesicular Glutamate Transporter-2: $p = 0.2009$; AChE: $p = 0.3118$, *Welch's t-test*).

The ratio of ipsilateral and contralateral projecting principal neurons was calculated from bilateral counts of projecting principal neurons from the most rostral to the most caudal LSO sections. The cell body had to be contained inside the fiber-lined border LSO border (principal and intrinsic neurons) or within approximately 100 μm of the LSO boundary (POs and shells). Cell position was plotted onto the outline of the LSO to create maps of cell projection patterns. Somatic silhouette area was calculated using *FIJI* software (Schindelin et al., 2012).

The methods for evaluating somatic and dendritic alignment and for confirming cellular alignment to the tonotopic axis are described in **Supplementary materials 3**, **4**, respectively. The cell body silhouette area, neuronal counts, angle difference between somatic long axis and dendritic vector, and orientation of LSO neurons to the tonotopic axis were subject to *Descriptive Statistics*, *Welch's t-test, and*

Two-way ANOVA using *Šídák's Multiple Comparison Test* ((Prism 9, GraphPad Software (2021), San Diego, CA, USA). *Note*: Statistical analyses that compare two cohorts tested for significance in *Prism* Software using the *Welch's t-test*; statical analyses comparing more than two groups were tested for significance using a *Two-way ANOVA* test. Means and standard deviations, *p-values*, and statistical tests are provided.

Results

The goal of this study was to begin a systematic description of some LSO circuits in the mouse in the context of various conflicting reports on the nucleus made in different mammalian species. We used a range of frequency-defined injection sites to describe the tonotopic relationship between principal cells of the LSO and the IC, applied quantitative methods to determine the laterality of these projections, and re-visited LSO cell categories with a focus on LOC efferents.

Labeling of principal and periolivary lateral superior olive neurons

Unilateral injections of the retrograde tracers, FD, FG, and/or AR, were made into the CNIC to label LSO neurons with ascending projections (**Figure 1**). Initially, pressure injections were made to get a global view of the connections, where unilateral injections labeled cells in both the ipsilateral and contralateral LSO (**Figure 1A**). The labeled neurons were distributed uniformly and appeared homogenous in appearance, except for some neurons on the border of the nucleus. The main neurons exhibited a general orientation toward the dorsal hilus (DH) and fit the descriptions of LSO principal neurons (Ollo and Schwartz, 1979; Cant, 1984). A small number of topographically labeled neurons were located on the border of the nucleus and often conformed to the border's shape; these matched the description of marginal cells (Ollo and Schwartz, 1979; Rietzel and Friauf, 1998). Cells with a larger cell body and dendrites that did not exhibit any particular orientation were occasionally labeled and found outside the LSO proper (**Figure 1A**, arrowheads). These were the PO neurons of the LSO as described in the cat (Adams, 1979, 1980).

Bilateral injections into the left and right CNIC labeled ipsilateral and contralateral LSO neurons side-by-side throughout the nucleus and were indistinguishable except by tracer (**Figure 1B**). Principal cells had elongated cell bodies of generally equal size (ipsilateral, 129.3 ± 37.37 μm^2; contralateral 131.2 ± 36.87 μm^2, **Supplementary Table 3**) with a marked orientation toward the DH. No neurons were double labeled, indicating that a single neuron did not give rise to an ascending axon that innervated both ICs. A much smaller
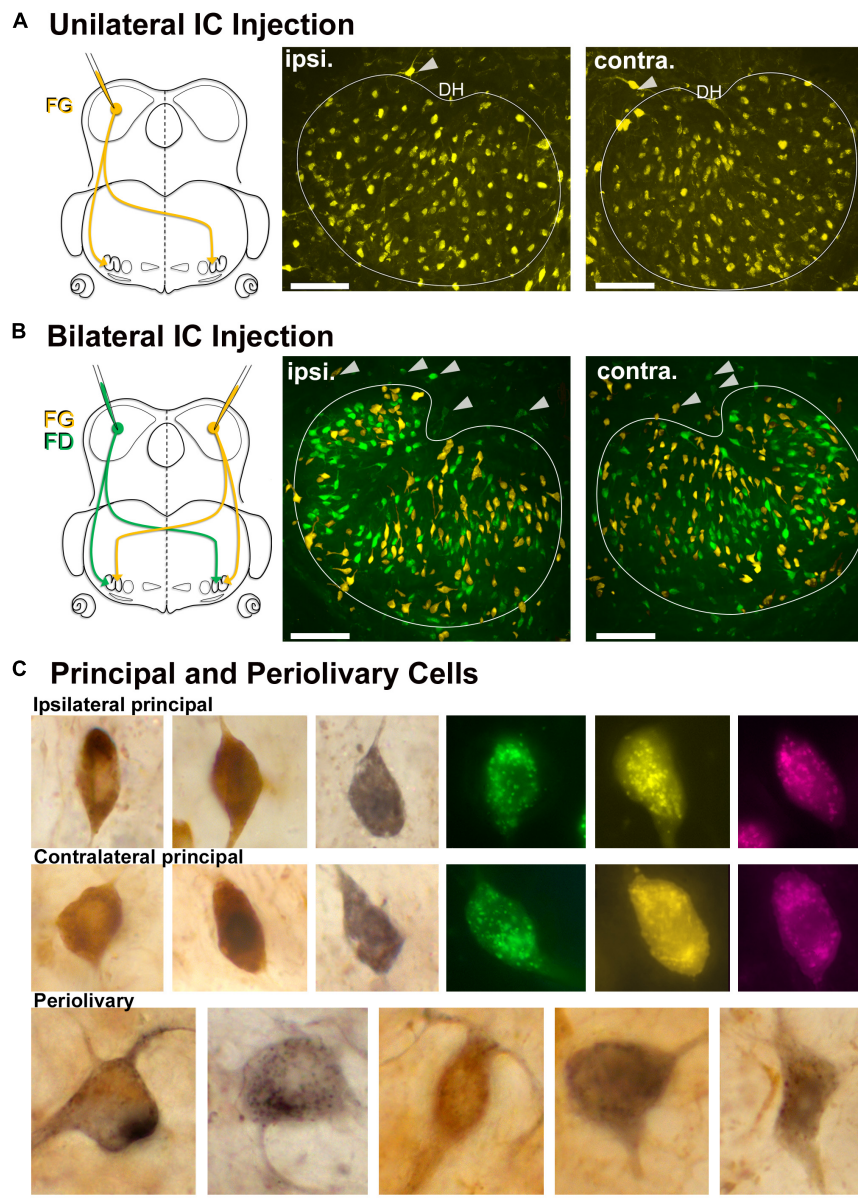
FIGURE 1

Retrogradely labeled LSO principal neurons from unilateral and bilateral tracer injections into the CNIC. **(A)** A unilateral injection of a retrograde tracer into the CNIC resulted in bilateral labeling of LSO principal neurons. Schematic representation of FluoroGold (FG) injected into the CNIC to label the neurons in the LSO with ascending projections. Photomicrographs (20x objective) of the ipsilateral and contralateral LSO showing FG-labeled principal neurons. *Gray arrowheads:* PO neurons on the borders of the LSO. **(B)** Schematic illustration of the retrograde tracers FG (yellow) and FD (green) injected into the right and left IC, respectively (same animal), to label the principal neurons in the LSO. Photomicrographs (20x objective) of the ipsilateral and contralateral LSO showing FG and FD labeled principal neurons in the same nucleus. *Gray arrowheads:* PO neurons on the borders of the LSO. **(C)** Photomicrographs (100x objective) of the ipsilateral (top row) and contralateral (middle row) principal cells labeled from chromogenic development of FG with DAB (brown) or NiDAB (black) and fluorescent tracers (FD-green, FG-yellow, Antonia Red-magenta). The principal neurons were fusiform with unipolar or bipolar dendritic extensions. The preolivary neurons were also labeled (bottom row) and featured a large, polygonal cell body using chromogenic development. ipsi., ipsilateral; contra., contralateral; FG, fluorogold; FD, fluorescein dextran. Scale bar equals 100 μm **(A,B)**, 25 μm **(C)**. The image approval for our adaptation of Stiebler and Ehret (1985) from John Wiley and Sons *via* the Copyright Clearance Centre; license number 5402831110296.

number (<25) of large, multipolar PO cells (198.5 $\pm$ 30.2 μm^2, Table 1) were labeled by all IC injections, and these were scattered around the outside of the LSO (Figures 1A,B).

A comparison of ipsilateral and contralateral principal cell body size and shape can be made and considered with respect to that of POs (Figure 1C).

TABLE 1 Cell body silhouette area (μm2) for the principal and periolivary (PO) neurons and the intrinsic and shell efferent neurons.

Neurons	Principal	PO	Intrinsic	Shell	Large CV
Number of cases	3	3	4	4	2
Number of cells	439	41	261	33	166
Median (μ m^2)	117.9	199.8	96.61	155.2	107.7
Mean (μ m^2) $\pm$ Standard deviation	123.9 $\pm$ 26.56	198.5 $\pm$ 30.17	97.33 $\pm$ 26.27	161.1 $\pm$ 28.26	111.8 $\pm$ 37.00

Two-way testing was used to compare the soma silhouette area of all subtypes of LSO neurons assessed in this study. A two-way ANOVA showed significant differences existed between the principal, PO, intrinsic, and shell neurons, but no significant difference occurred between the CV labeled neurons and the principal neurons [$F(105,438) = 0.86$, $p = 0.8408$] or the CV labeled neurons and the intrinsic efferents [$F(1,103) = 3.09$, $p = 0.0816$].

Labeling of lateral olivocochlear efferents

Lateral olivocochlear efferents were labeled by pressure injections of the retrograde tracers FD, FG, or CTB into the round window of the cochlea (**Figure 2A**). The labeling for intrinsic efferents, found within the LSO proper, was entirely ipsilateral. Labeled cells were oval with thin unipolar or bipolar dendritic stalks generally evident on opposite poles. The intrinsic efferents appeared to align perpendicularly to the borders of the LSO nucleus. Their somata were slightly smaller (97.33 ± 26.27 μm^2, **Table 1**) than those of principal cells but their shape was roughly the same (**Figures 2A,B**, row 1). A few labeled shell efferents were found bilaterally and outside the LSO borders, often near the DH (**Figure 2A**, arrowheads). Shell neurons were larger than intrinsic neurons (average area, 161.1 ± 28.3 μm^2, **Figure 2B**, bottom row and **Table 1**).

ChAT or AChE was used to determine total efferent cell distribution (**Figure 3A**) as well as cell morphology (**Figure 3B**) because they had previously been shown to label LOC efferents in the mouse (Safieddine et al., 1997; Brown, 2011). Intrinsic cells were orientated in line with the tonotopic axis of the LSO (**Figure 3A**) as previously reported (Vetter and Mugnaini, 1992; Brown, 2011). ChAT and AChE staining confirmed that the two methods exhibited equal sensitivity for counting (ChAT: average total, 362.0 ± 25.41; AChE: average total, 357.8 ± 18.63; $p = 0.7532$; **Table 2**) and size measurements (**Supplementary Table 3**). Intrinsic efferents had fusiform-shaped cell bodies and the dye often extended into the primary dendrite (**Figure 3B**, top row). The labeling of the intrinsic and shell neurons with cholinergic staining was consistent with the LOC efferents labeled by retrograde tracers (**Figure 3**).

Double labeling experiments were used to reveal principal and intrinsic neurons within the same mouse. An injection of one tracer into the CNIC and an injection of a second tracer into the cochlea on the opposite side permitted direct side-by-side comparisons of principal and intrinsic neurons (**Figure 4A**). Principal neurons were distributed bilaterally throughout the LSO. In contrast, the intrinsic neurons were unilateral to the cochlear injection and tended to avoid the border of the nucleus. No neuron was double labeled, indicating that no neuron gave rise to a branched axon that innervated the separate targets.

When tissue was stained only by CV, it was impossible to distinguish principal from intrinsic cells (**Figure 4B**). The PO and shell neurons were observed scattered around outside the LSO borders and were always found in association with retrogradely labeled principal and intrinsic neurons, respectively (**Figure 4C**).

Topographic connections between lateral superior olive principal cells and the central nucleus of the inferior colliculus

Thirteen mice received iontophoretic injections of a retrograde tracer into the CNIC at an identified frequency location (**Supplementary Figure 1**). Four representative cases are shown to illustrate the topography and the bilateral symmetry in the projection (**Figure 5**). Plots from three adjacent sections were transferred onto the section representing the 50th percentile. The labeled cells occupy a relatively circumscribed region in the LSO. In terms of topography, note how the progressively deeper IC injections with higher frequencies (**Figures 5**, left column, **6A**) create labeling of principal cells in the LSO that move e*n masse* as a "stripe" from lateral to medial (**Figures 5**, middle columns, **6B**). There is also a scattering of labeled PO neurons found just outside the LSO, and these occur in predictably low numbers but in variable locations. The pattern of labeling was similar for all cases and independent of the retrograde tracer used, involving principal, marginal, and PO cells.

The bilateral symmetry of the retrograde labeling was assessed by copying the plot from right 50th percentile of the LSO, flipping the image in the horizontal plane, and then superimposing the flipped image onto the original left LSO (**Figure 5**, far right column). The mirror imaging of the right and left plots confirms the symmetry. The spatial balance was also evident by the equal numbers of ipsilateral and contralateral labeled cells whose ratio averaged 1.05 ± 0.16 (**Table 3**).

While the "sheets" of labeled cells exhibit a tonotopic organization, there is also spatial overlap of principal cells that exhibited separate but similar frequency characteristics (**Figure 6B**). This overlap of labeled cells in the LSO reflects the
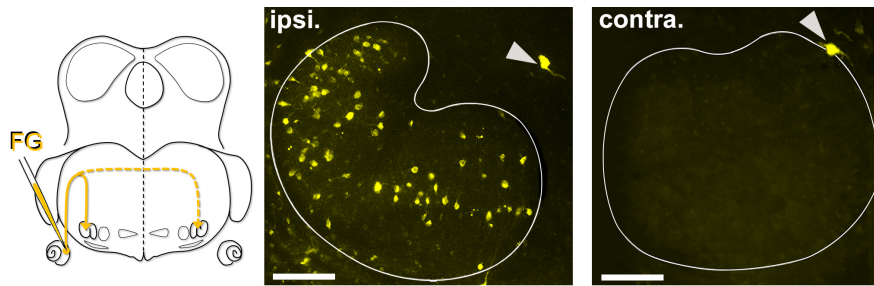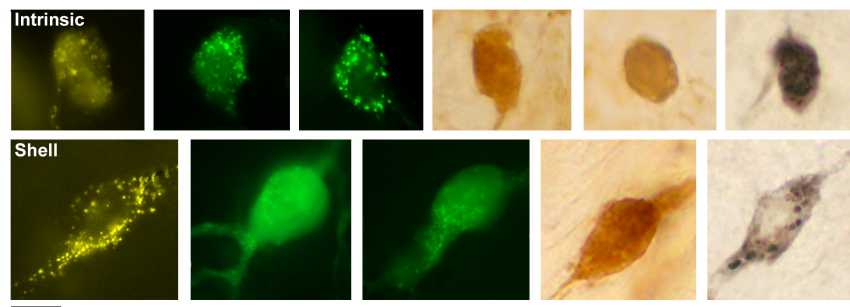
FIGURE 2
Labeled lateral olivocochlear (LOC) efferents following retrograde tracer injections into the cochlea. **(A)** Schematic illustration of retrograde tracer injected through the round window of the left cochlea. Solid yellow line indicates the primary pathway to the ipsilateral LOCs, whereas the dashed line leads to the very few contralateral LOCs. *Gray arrowheads:* shell neurons on the borders of the LSO. **(B)** Photomicrograph (100x objective) of the intrinsic LOC efferents (top row) labeled with chromogenic development (DAB-brown, NiDAB-black) and with fluorescent markers (FG-yellow, FD-green). The intrinsic neurons were small and round, and look similar to the principal neurons. The shell neurons (bottom row) were labeled in the same tissue as the intrinsic neurons, and featured a large cell body with broader dendritic extensions. ipsi., ipsilateral; contra., contralateral; FG, fluorogold; FD, fluorescein dextran. Scale bar equals 100 μm **(A)**, 25 μm **(B)**. The image approval for our adaptation of Stiebler and Ehret (1985) from John Wiley and Sons *via* the Copyright Clearance Centre; license number 5402831110296.

overlap observed in the IC injection sites having different but nearby frequency characteristics (**Figure 6A**). The spatial spread in the distribution of labeling may be a result of combining data from different cases onto a model LSO. PO cell labeling was relatively invariant, regardless of the location of the IC injection (**Figure 5**, middle columns). Every part of the CNIC appears innervated by both populations of cells with principal and marginal cells having restricted projections and PO cells having widespread projections.

Tonotopic axis

The angle of the somatic long axis compared to the corresponding angle of its dendritic vector for principal and intrinsic neurons was small, indicating alignment of these two features: (principal cells: $7.24 \pm 10.42°$; intrinsic efferents: $6.49 \pm 9.33°$; **Supplementary Table 4**). This result inferred that the cell body pointed in the direction of the dendritic trajectory (further details in **Supplementary material 3**) and allowed us to quantify the somatic orientation of LSO cells to the tonotopic axis (**Supplementary material 4**).

The principal cells created a columnar profile that defined an "isofrequency" sheet (**Figures 5**, **6B**) that ran the length of the LSO, hinged near the DH. An isofrequency sheet for each case was laid out on the 50th percentile of the nucleus (**Figure 6C**). A centroid was calculated for each isofrequency sheet (FIJI) and black vertical lines were drawn through the centroids to create a long axis line for each sheet (**Figure 6C**). The centroids were connected by a black line that represented the tonotopic axis of the nucleus (**Figure 6D**).

The Hamilton–Jacobi Skeleton algorithm (He et al., 2021), which bisects a complex structure by following the curvature of the opposing borders, was used to create a representative tonotopic axis line for 14 LSO sections (**Figure 6D**, red lines). This output closely matched the tonotopic axis defined by us [**Figure 6D**, black line; *Welch's test* ($p = 0.2967$)]. The spatial representation of different isofrequency regions appear uniformly distributed across the LSO, at least up to 60 kHz, suggesting no augmented frequency representation. A line through the 30 kHz region would essentially bisect the LSO into lateral and medial halves.

TABLE 2 Counts comparing the distribution of LOC efferents stained by AChE or ChAT.

Case	Stain	Count
AM4	AChE	343
AM5	AChE	344
AM11	AChE	389
AM298	AChE	331
AM1348	ChAT	385
AM1351	ChAT	380
AM1353	ChAT	382
AM1417	ChAT	376
AM1419	ChAT	331
AM1450	AChE	354
AM1454	AChE	355
AM1477	ChAT	349
Average AChE	357.8 ± 18.63	
Average ChAT	362.0 ± 25.41	
Combined average	359.9 ± 21.35	

The number of LOC efferent neurons were calculated to compare the labeling distribution between the two stains. The average count for AChE and average count for ChAT were not significantly different ($p = 0.7532$).

The somatic long axes of principal and intrinsic neurons were placed onto our LSO model (**Supplementary material 4**) and the intersecting angle θ was measured with respect to the tonotopic axis. As suggested from the literature, LSO neurons are expected to be oriented at right angles to the tonotopic axis (Scheibel and Scheibel, 1974; Friauf et al., 2019). Each angle was reported as an absolute value and subtracted from 90°. Principal and intrinsic neurons exhibited a somato-dendritic orientation that aligned to one another and was mostly orthogonal to the tonotopic axis (**Figure 7**; principal neuron mean of all LSO sections = 32.99 ± 24.55°; intrinsic neuron mean = 29.70 ± 22.51°). The arrangement was not perfect but the tendency was definitely present. The PO neurons and shell efferents, however, exhibited somato-dendritic morphology that did not contribute to the structural laminae (middle, PO mean = 61.28 ± 24.62°; shell efferent mean = 59.71 ± 24.39°, **Supplementary Table 5**). These measurements confirmed the more orthogonal appearance of these two cell types with respect to the tonotopic axis of the LSO.

Discussion

The present study provides a qualitative and quantitative anatomical assessment of four types of LSO projecting neurons with connections with the IC or cochlea. Retrograde tracers placed into the CNIC labeled neurons with ascending projections (principal and PO neurons), whereas neurons with descending projections were labeled by injections of retrograde tracers deposited into the cochlea or with cholinergic markers (intrinsic and shell LOC efferents). The projection laterality of the principal neurons to the IC was determined by comparing the number of ipsilateral and contralateral labeled neurons from unilateral IC injections and found to be essentially equal. The tonotopic alignment of the four subtypes of LSO neurons was examined and quantified to develop ideas about frequency specificity and possible frequency enhancement with regard to connections between the LSO and the IC. Features of somatic morphology were established to supplement connectivity data and to help distinguish principal and intrinsic neurons. These data are summarized in **Figure 8**.
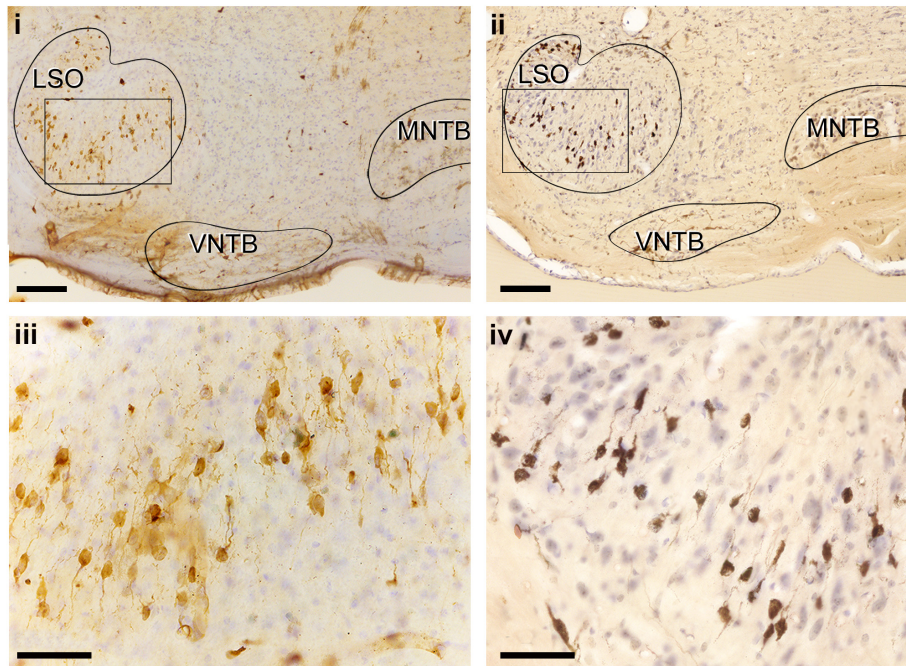
In the mouse, principal and intrinsic neurons are spatially intermixed and have similar somatic size, shape, and dendritic morphology. Collectively, these neurons give the LSO a laminar texture and are structurally specialized to receive restricted input, which endows each with a well-defined receptive field. These cells are typical of classic lemniscal sensory neurons (Calford et al., 1983; He, 2003; Anderson and Linden, 2011).

Lateral superior olive principal neurons: Projection symmetry and topography

Lateral superior olive cells have been divided into separate categories based on soma-dendritic features, cell body size, and location within the LSO nucleus (Ollo and Schwartz, 1979; Cant, 1984; Rietzel and Friauf, 1998), chemical markers (Helfert et al., 1989; Eybalin, 1993) or projections (Adams, 1979; Glendenning and Masterton, 1983; Henkel and Brunso-Bechtold, 1993). There is general agreement as to the main types of neurons—principal, periolivary, intrinsic, and shell—but not for all. The previously mentioned marginal cells, with their bipolar appearance and topographic relationship with the IC, may simply be principal cells that lie on the borders of the LSO (Ollo and Schwartz, 1979; Rietzel and Friauf, 1998). Bipolar, unipolar, and banana-like cells of the rat exhibit disk-shaped dendritic trees and may also represent different subgroups of principal cells with variations in location and chemistry (Rietzel and Friauf, 1998). LSO cell taxonomy is confounded by observations drawn from different species of different ages using different methods. The resolution of cell types will ultimately depend on their physiological properties and the nature of the synaptic circuits to which they belong.

We demonstrated a strict topographic projection from the LSO to the IC, which augmented previous but less detailed reports in cats and rats (Brunso-Bechtold et al., 1981; Kelly et al., 1998). Our isofrequency layers of the IC closely corresponded to tonotopic maps where isofrequency lines were drawn by connecting points of common frequencies
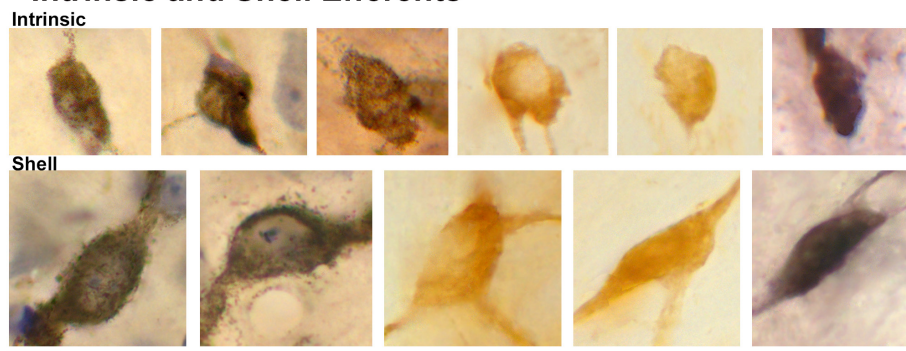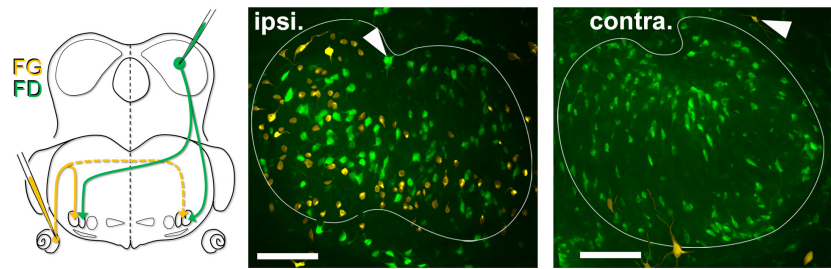
FIGURE 3

Labeled cholinergic LOC efferent neurons. LOC neurons were labeled using cholinergic markers, ChAT and AChE, and counterstained with CV. **(Ai)** Photomicrograph (10x objective) of the superior olivary complex (SOC) region labeled by ChAT immunostaining. **(ii)** Photomicrograph (10x objective) of the SOC region labeled by AChE staining. **(iii,iv)** Higher magnification micrographs (40x objective) of inset **(i,ii)**, showing the ChAT and AChE labeled LOC neurons contained within the LSO, respectively. Note the similarity of ChAT and AChE labeling. **(B)** Photomicrographs (100x objective) showing the cholinergic LOC neurons labeled from either ChAT or AChE staining. The intrinsic neurons (top row) feature fusiform somata and were distributed throughout the core of the LSO nucleus. The shell neurons (bottom row) were larger and more globular in shape. LSO, lateral superior olive; VNTB, ventral nucleus of the trapezoid body; MNTB, medial nucleus of the trapezoid body. Scale bar equals 250 μm **(Ai,ii)**, 50 μm **(Aiii,iv)**, 25 μm **(B)**. The image approval for our adaptation of Stiebler and Ehret (1985) from John Wiley and Sons *via* the Copyright Clearance Centre; license number 5402831110296.

(Stiebler and Ehret, 1985; Portfors et al., 2011). The congruency of these isofrequency layers is remarkable given that these maps were generated years apart by different methods, using different mouse strains, exposed to surgical perturbations and electrode penetrations, and subject to tissue stress by histological processing (Supplementary material 5).

Following our frequency-guided unilateral IC injections, there are unlabeled cells among the frequency-dependent labeled cells. Some of the unlabeled cells would be principal cells projecting to the other IC and others would be intrinsic efferents. Still others could have projections to different nuclei such as the nuclei of the lateral lemniscus, AVCN and dorsal cochlear nucleus (Browner and Webster, 1975; Glendenning et al., 1981; Glendenning and Masterton, 1983). There was also more spatial overlap of cells from different frequency zones than expected when combining data from different

FIGURE 4

Double injection of retrograde tracers into the right IC and left cochlea to label the LSO neurons with ascending projections and LOC efferents with descending projections, respectively. LSO neurons with ascending and descending projections were labeled *via* tracer injections of FD into the right CNIC and FG into the round window 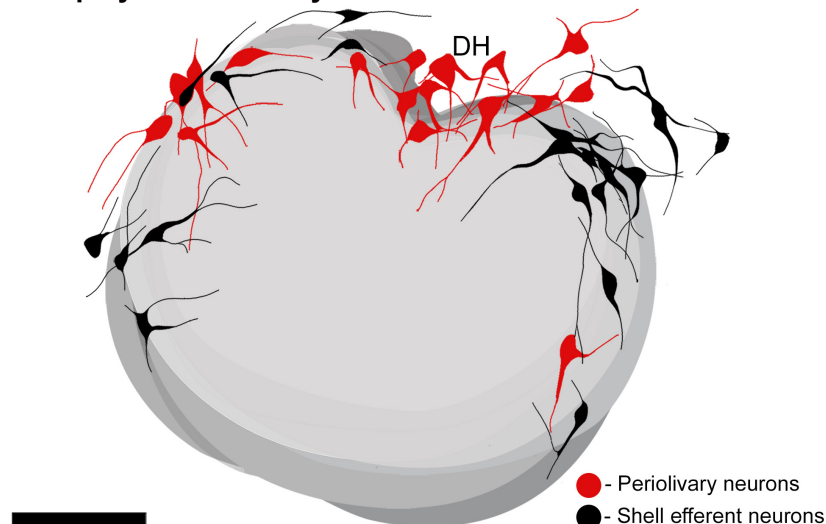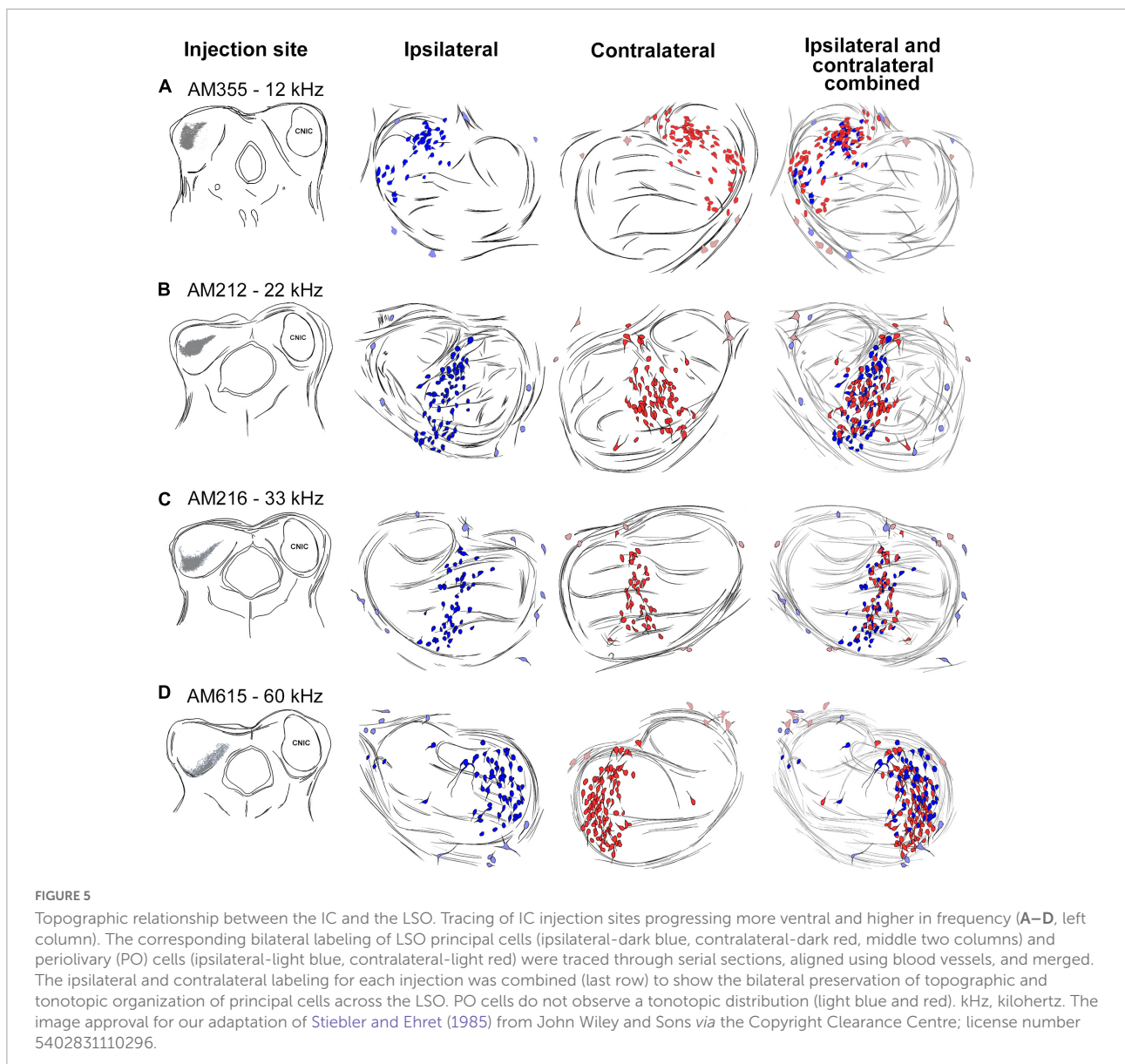of the left cochlea, respectively. **(A)** Schematic illustration of the injection sites and pathways for the projecting neurons. Fluorescent micrograph showing the left LSO containing labeled contralateral principal neurons (FD-green) and ipsilateral LOC efferents (FG-yellow). The LOC efferents were primarily ipsilaterally projecting, with only a few shell neurons projecting contralaterally. *Gray arrowheads:* PO neurons (green fluorescence) and shell neurons (yellow fluorescence) on the borders of the LSO. **(B)** Photomicrographs (100x objective) of CV labeled LSO neurons. In tissue stained by CV, we were unable to distinguish principal from intrinsic neurons due to the similarity in size and shape. **(C)** Summary of location of labeled periolivary and shell neurons around the borders of the LSO. The position of PO (red) and shell (black) neurons are shown collapsed across 18 LSO sections to illustrate their spatial distribution around the LSO. ipsi., ipsilateral; contra., contralateral; FG, fluorogold; FD, fluorescein dextran. Scale bar equals 100 μm **(A,C)**, 25 μm **(B)**. The image approval for our adaptation of Stiebler and Ehret (1985) from John Wiley and Sons *via* the Copyright Clearance Centre; license number 5402831110296.

cases onto an LSO model. These border irregularities might simply reflect the combining of data across different animals. Alternatively, they could imply that the system is inherently noisy because it reflects the naturally occurring acoustic environment. That is, we rarely, if ever, encounter pure tones. Rather, we hear complex sounds such as speech, with time-varying frequencies and amplitudes, in the presence of random noises, all occurring at once and from different sources. Could it be that sound perception and discrimination are learned probability functions rather than a precise hard-wired process like the keyboard of a piano? Maybe topographic brain maps are only approximate blueprints for brain function: the auditory world is uniquely created for each individual animal by populations of neurons that learn to work together over time.

FIGURE 5

Topographic relationship between the IC and the LSO. Tracing of IC injection sites progressing more ventral and higher in frequency (**A–D**, left column). The corresponding bilateral labeling of LSO principal cells (ipsilateral-dark blue, contralateral-dark red, middle two columns) and periolivary (PO) cells (ipsilateral-light blue, contralateral-light red) were traced through serial sections, aligned using blood vessels, and merged. The ipsilateral and contralateral labeling for each injection was combined (last row) to show the bilateral preservation of topographic and tonotopic organization of principal cells across the LSO. PO cells do not observe a tonotopic distribution (light blue and red). kHz, kilohertz. The image approval for our adaptation of Stiebler and Ehret (1985) from John Wiley and Sons *via* the Copyright Clearance Centre; license number 5402831110296.

Their frequency preference is acquired by their relative position in the auditory system and refined by experience but perhaps not dictated entirely by innate and immutable frequency-specific responses.

The pattern of labeled neurons in the ipsilateral and contralateral LSO following a unilateral injection of a retrograde tracer into the mouse IC was not only topographic but also symmetric. If we assume that ipsilateral and contralateral projecting neurons have similar uptake and transport efficiency for detectability, then we could anticipate that the ratio of ipsilateral versus contralateral projecting cells, regardless of the size of the injection, ought to be stable, at least for injections contained within the same IC subdivisions. On average, an equal number of labeled principal cells were reliably observed in each LSO from a unilateral injection in the CNIC (1.05 ± 0.16). The gerbil, in spite of considerable variability, exhibited a similar mean ratio (0.94 ± 0.59, Mellott et al., 2021) consistent with qualitative conclusions made for cats (Adams, 1979), ferrets (Henkel and Brunso-Bechtold, 1993), and rats (Beyerl, 1978; Fredrich et al., 2009). Other researchers reported differences in ipsi- versus contra-projections and these could be due to species differences or methods. Part of the difference could also be that the tracers being used currently are significantly more sensitive than horseradish peroxidase, which was used in many of the older publications.

The neurons lying outside the LSO with larger somata, multipolar dendrites, and ascending projections to the IC are
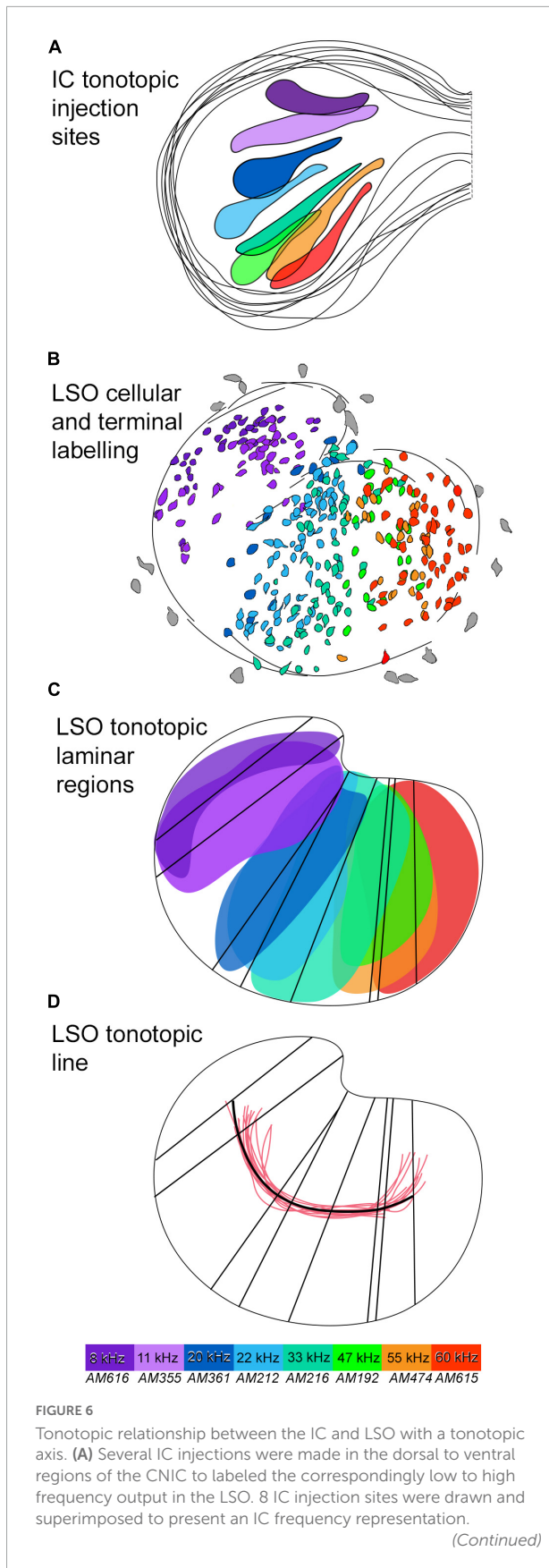
FIGURE 6 (Continued)

Frequencies included: 8, 11, 20, 22, 33, 47, 55, and 60 kHz (color coded). **(B)** The corresponding label of principal neurons in the LSO, color coded to match. The labeled principal cells show the LSO low to high frequency organization progressing from the lateral to medial limb, respectively. **(C)** The corresponding LSO neurons labeled from each IC injection were color coded. A region for each color of principal cells representing one frequency was drawn by outline the area of labeled cells to form a lamina for each frequency. A line representing the long axis of each frequency region was drawn to represent an isofrequency line. **(D)** A line (black) representing the tonotopic axis was drawn by connecting centroids of all the isofrequency lines and was compared to other tonotopic axis lines (red) derived from the Hamilton Jacobi output from other LSO sections. A color map is included, with purple corresponding to labeled elements from 8 kHz, and red corresponding to the highest frequency elements of 60 kHz. IC, inferior colliculus; LSO, lateral superior olive; kHz, kilohertz. The image approval for our adaptation of Stiebler and Ehret (1985) from John Wiley and Sons *via* the Copyright Clearance Centre; license number 5402831110296.

analogous to the PO neurons in cats (Adams, 1979, 1980) and gerbils (Schofield and Cant, 1992). POs tended to be concentrated around the DH but could be found anywhere in the vicinity of the LSO and connected to the ipsilateral or contralateral IC but not to both. Some members of this population labeled with every IC injection but their numbers were relatively low and their location unpredictable. This pattern of labeling suggested a diffuse projection to the IC and their widely branching dendrites seemed suited to intercept input from a wide swath of incoming fibers.

The POs represent what had been called isodendritic neurons commonly found in the brain stem reticular system or the intralaminar (posterior) nuclei of the thalamus (Ramon-Moliner, 1962; Morest, 1964; Scheibel and Scheibel, 1966; Lu et al., 2009). Such cells receive anatomically heterogeneous input from the spinal cord and medial lemniscus (Lund and Webster, 1967; Malmierca et al., 2011), demonstrate wide receptive field properties (Wepsic, 1966; Erickson et al., 1967; Aitkin, 1973), exhibit distinct neurochemical differences (Lu et al., 2009), and have been considered part of a multimodal pathway for integrative functions (Liu et al., 2022). Could POs be part of the non-lemniscal sensory system? Regardless, these anatomical data imply sensitivity to a range of different kinds of inputs and projections that exert a more modulatory upstream influence.

Labeling of lateral superior olive neurons with descending projections

Intrinsic neurons of the mouse exhibit bipolar morphology that resembles that of the principal neurons. They have also been shown to have restricted terminations in the inner hair cell region of the ipsilateral cochlea (Warr et al., 1997). In

FIGURE 6

Tonotopic relationship between the IC and LSO with a tonotopic axis. **(A)** Several IC injections were made in the dorsal to ventral regions of the CNIC to labeled the correspondingly low to high frequency output in the LSO. 8 IC injection sites were drawn and superimposed to present an IC frequency representation.

(Continued)

TABLE 3   Counts comparing the distribution between the ipsilateral and contralateral principal neurons of five cases.

Case	Tracer	Total ipsilateral cells	Total contralateral cells	Total count	Ratio
AM1360	FD	362	350	712	1.03
AM1362	FD	812	685	1497	1.18
AM1496	FD	273	232	505	1.17
AM1496	FG	370	382	752	0.969
AM1507	FD	203	263	466	0.772
AM1507	FG	743	589	1332	1.26
AM1526	FG	160	160	320	1

The number of ipsilateral and contralateral principal neurons were calculated to compare the labeling distribution between both sides. The ratio was computed by dividing the total ipsilateral cells of each case by the total contralateral cells. A ratio closest to 1, infers a labeling distribution that is most comparable between the two sides. The average ratio for these seven cases is 1.05 ± 0.16. Cases mentioned more than once were double labeled with FD and FG tracers.

contrast, shell neurons have larger cell bodies and exhibit multipolar, radiating dendrites. Importantly, evidence supports the notion that shell neurons give rise to branching axons with generally a bidirectional course along the cochlear spiral with *en passant* and terminal swellings extending a tonotopic range of 1–2 octaves (Brown, 1987, 1993; Warr et al., 1997). The diffuse and expansive projections of shell neurons are consistent with characteristic attributed to polysensory, non-lemniscal cells (Morest, 1964; Hu, 2003; Kimura et al., 2003; Komura et al., 2003; Anderson and Linden, 2011).

Long-term acquired hearing loss does not affect the size, number, or ratio of ipsilateral:contralateral projecting OC efferent neurons when comparing CBA/CaH, DBA/2 and shaker-2 (sh2/sh2) mice at 6 months of age (Suthakar, 2016). Both DBA/2 and sh2/sh2 mice exhibited ABR thresholds exceeding 100 dB SPL at this age. From these observations and the relatively short post-surgical survival of our animals, we infer that our tracer injections into the cochlea did not alter the somatic structure of auditory efferents as seen through a light microscope.

Considerations of lateral superior olive laminar organization and tonotopy

The concept of a laminar organization of auditory structures (Rockel and Jones, 1973) fostered the idea for a topologic representation of isofrequency layers that underpinned tonotopy (Boudreau and Tsuchitani, 1970; Aitkin and Webster, 1971; Guinan et al., 1972; Merzenich and Reid, 1974; Bourk et al., 1981; Imig and Morel, 1985; Friauf and Ostwald, 1988; Banks and Smith, 1992; Ryugo and May, 1993; Sommer et al., 1993; Spirou et al., 1993; Doucet and Ryugo, 2003; Malmierca et al., 2005; Muniak et al., 2013; Gómez-Álvarez and Saldaña, 2015). Previous studies utilized qualitative observations with Golgi staining to label the extensive dendritic branches of LSO neurons and suggested a laminar organization that appeared perpendicular to the tonotopic axis (Ramón y Cajal, 1909; Scheibel and Scheibel, 1974; Cant, 1984; Helfert and Schwartz,
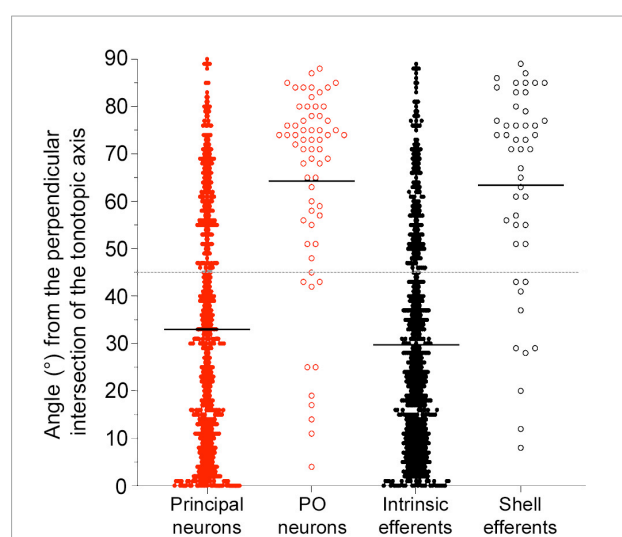

FIGURE 7

Plot of the angles for LSO neurons with ascending (red) or descending (black) projecting axons with respect to the tonotopic axis. Angle measurements for the four types of LSO neurons are shown and combined from three regions of the LSO (rostral, middle, and caudal sections). The average angle (black line) was presented for all subtypes. *Gray dashed line:* 45-degree threshold. Principal and intrinsic neurons illustrate similar angle deviations, with mean alignment below the 45-degree threshold across all planes. Periolivary (PO) neurons and shell efferent neurons both had values above the 45-degree threshold for all planes. Smaller values indicate alignment with the frequency organization. PO, periolivary. The image approval for our adaptation of Stiebler and Ehret (1985) from John Wiley and Sons *via* the Copyright Clearance Centre; license number 5402831110296.

1987; Vetter and Mugnaini, 1992; Henkel and Brunso-Bechtold, 1998; Gómez-Álvarez and Saldaña, 2015). The utility of quantitative analyses using vectors and angles demonstrated a laminar organization of LSO neurons in the human (Kulesza, 2007) and a non-laminar organization of MOC neurons in the mouse (Brown and Levine, 2008). We extended these observations by showing principal and intrinsic neurons conform to the laminar organization of the LSO, whereas PO
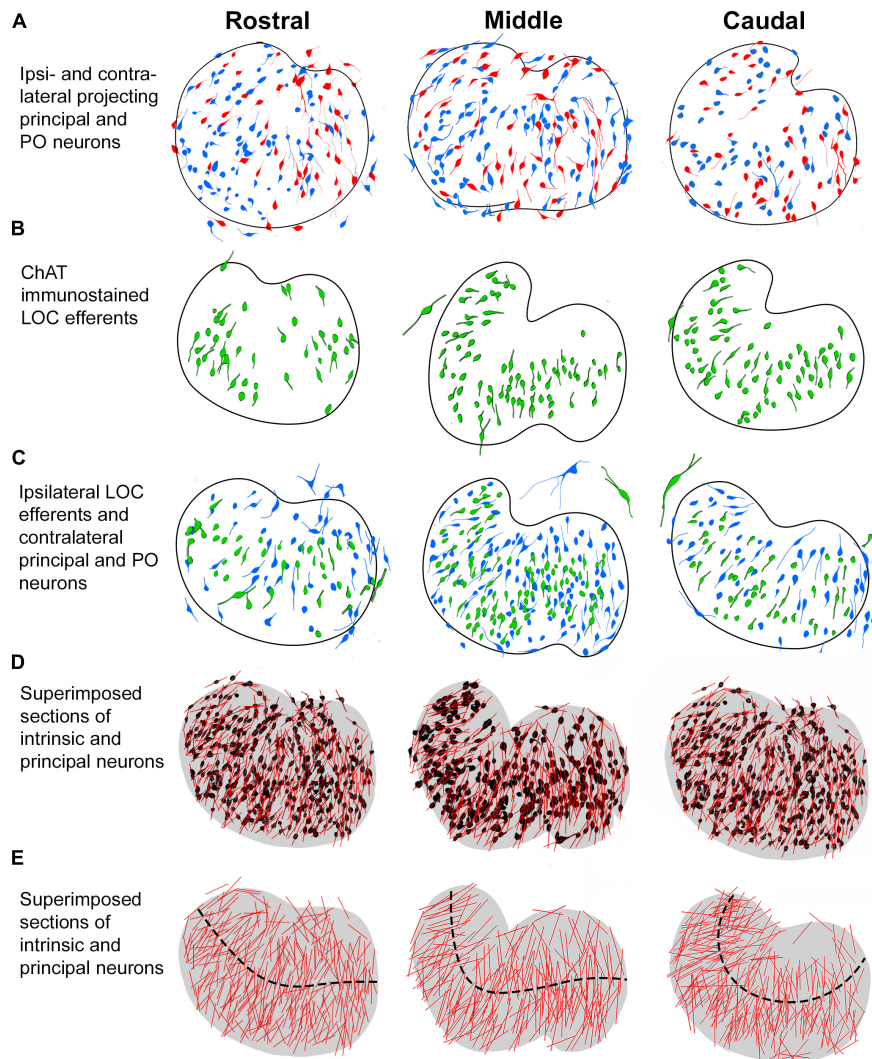
FIGURE 8
Summary of labeling pattern of principal and intrinsic neurons in rostral, middle, and caudal LSO sections. The projecting cell types were traced and mapped to illustrate their distribution in representative anterior-posterior regions of the nucleus. **(A)** Ipsilateral (red) and contralateral (blue) principal neurons labeled from bilateral CNIC injections. **(B)** Intrinsic efferent neurons labeled by ChAT immunostaining (green). **(C)** Contralateral projecting principal neurons (blue) and ipsilateral projecting intrinsic neurons (green) labeled by retrograde tracer injections into the CNIC and cochlea, respectively. The larger neurons on the borders of the LSO are identified as the PO and shell neurons (seen in **A–C**). **(D)** LSO neurons with ascending or descending projections labeled from separate LSO sections were superimposed and collapsed as one color (black) on a representative rostral, middle, and caudal LSO section. The somatic long axis line (red) is contrasted against the individual neurons. **(E)** A model LSO representing rostral, middle, and caudal sections was drawn (gray, fourth row). Here, the relative alignment of principal and intrinsic neurons are shown with the representative tonotopic axis (black dashed line). An overall organization within the nucleus is seen to comprise fibrodendritic laminae. PO, periolivary; LOC, lateral olivocochlear. The image approval for our adaptation of Stiebler and Ehret (1985) from John Wiley and Sons via the Copyright Clearance Centre; license number 5402831110296.

and shell neurons do not. The observation that MOCs are sharply tuned (Liberman and Brown, 1986) even though they are multipolar with radiating dendrites (Brown and Levine, 2008) implies that frequency-specific inputs are concentrated on the cell body or proximal dendrites, not along the entire dendritic domain.

In the LSO, principal cells contribute to the isofrequency organization and are sharply tuned (Guinan et al., 1972;

Tsuchitani, 1977; Sanes and Rubel, 1988; Tollin and Yin, 2002). In the LSO of the mouse, principal and intrinsic neurons adopt a strict laminar organization. On this basis, we predict that LOC neurons will exhibit sharp frequency tuning like that of LSO principal cells, although physiological recordings have not yet been made from LOC neurons. Another enigma about LOCs is that in many species, they are located outside of the LSO (Warr, 1975; Thompson and Thompson, 1986). The predominantly

ipsilateral projecting efferents in the squirrel monkey have small, round-oval somata that could represent LOCs. The elongated neurons that exhibited bilateral projections were embedded in surrounding fibers of the SOC (Thompson and Thompson, 1986); their projection pattern and fibrodendritic alignment make them candidates for the sharply tuned MOCs.

Comparative issues of the lateral superior olive

There is no uniform agreement with respect to the neurochemistry of LSO neurons, due in part to species variations in cellular composition, cell body versus terminal staining, age of animals studied, and history of noise exposure (Helfert et al., 1989; Vetter et al., 1991; Vetter and Mugnaini, 1992; Eybalin, 1993; Kandler et al., 2002; Maison et al., 2002; Nabekura et al., 2003; Niu et al., 2004; Jenkins and Simmons, 2006; Wu et al., 2020). For the cat and guinea pig, the LSO cell population seems to be almost equally divided between excitatory and inhibitory cells (Helfert et al., 1989; Glendenning et al., 1992). In the gerbil, 75% of the LSO cells are reported to be glutamatergic (Mellott et al., 2021). The projections of LSO principal neurons to the IC have been considered a key to understanding the role of excitation and inhibition in the process of binaural interactions but there is disagreement concerning many of the very basic issues of the circuitry. Different species exhibit variable immunochemical properties of LSO neurons and variations in the laterality of projections with respect to frequency and transmitter (Glendenning and Masterton, 1983; Saint Marie et al., 1989; Saint Marie and Baker, 1990; Finlayson and Caspary, 1991; Glendenning et al., 1992; Henkel and Brunso-Bechtold, 1993; Brunso-Bechtold et al., 1994; Oliver, 2000). Projections of the LSO to the IC are not distinguishable by glycinergic or glutamatergic features alone (Fredrich et al., 2009; Mellott et al., 2021). Sorting out the details of these projections in different species will be important to understand the cellular mechanisms of binaural level processing and warrants separate studies that focus on excitation and inhibition by using pathway tracing, synaptic analyses, and markers for glycine and glutamate.

The mouse has primarily high frequency hearing, unlike that of the cat, ferret, chinchilla, gerbil, guinea pig, and human. It can therefore be predicted that there will be anatomical specializations associated with the animal's natural history, ecological niche, hearing range, and conspecific communication requirements. In rodents, for example, the known natural habitat of the gerbil is an underground burrow (Fisher and Llewellyn, 1978); it should not be surprising if its LSO differs from rodents living above-ground. In burrows, there is reduced propagation of high frequencies (Okanoya et al., 2018) and little opportunity for detecting lateralized sounds (Heth et al., 1986; Barker et al., 2021). It is, however, curious

that three burrowing rodents, the gerbil, mountain beaver, and naked mole rat, have vastly different audible hearing ranges (Merzenich et al., 1973; Heffner and Heffner, 1993; Okanoya et al., 2018). In comparison, the mouse lives in open fields and urban developments and has high frequency hearing to assist in conspecific communication and danger detection (Ehret and Riecke, 2001; Portfors and Perkel, 2014). Our results provide new quantitative details on the auditory anatomy of the mouse but emphasize the importance of comparative studies if we are to better our understanding of mammalian hearing.

Data availability statement

The original contributions presented in this study are included in the article/**Supplementary material**, further inquiries can be directed to the corresponding author.

Ethics statement

This study was reviewed and approved by the Garvan/St Vincent's Hospital Animal Ethics Committee. This study was performed in strict accordance with the Australian Code for the Care and Use of Animals for Scientific Purposes (2013) and the ethical guidelines of the National Health and Medical Research Council (NHMRC) of Australia. All animals were handled according to Animal Ethics Committee protocols (Animal Research Authority: 19-33, 20-02, and 21-13).

Author contributions

Funding

Acknowledgments

The authors thank Giedre Milinkeviciute, Michael A. Muniak, Kirupa Suthakar, and Valentina Vanghi for their technical contributions. The authors also extend their thanks to the reviewers for their constructive criticisms of this manuscript.

Conflict of interest

The authors declare that the research was conducted in the absence of any commercial or financial relationships that could be construed as a potential conflict of interest.

Publisher's note

All claims expressed in this article are solely those of the authors and do not necessarily represent those of their affiliated organizations, or those of the publisher, the editors and the reviewers. Any product that may be evaluated in this article, or claim that may be made by its manufacturer, is not guaranteed or endorsed by the publisher.

Supplementary material

The Supplementary Material for this article can be found online at: https://www.frontiersin.org/articles/10.3389/fncir.2022.1038500/full#supplementary-material

References

Adams, J. (1979). Ascending projections to the inferior colliculus. *J Comp. Neurol.* 183, 519–538. doi: 10.1002/cne.901830305

Adams, J. C. (1980). Crossed and descending projections to the inferior colliculus. *Neurosci. Lett.* 19, 1–5. doi: 10.1016/0304-3940(80)90246-3

Adobe Photoshop, C. S. (2021). *Classroom in a book*. Berkeley, CA: Peachpit Press.

Aitkin, L. M. (1973). Medial geniculate body of the cat: Responses to tonal stimuli of neurons in medial division. *J. Neurophysiol.* 36, 275–283. doi: 10.1152/jn.1973.36.2.275

Aitkin, L. M., and Webster, W. R. (1971). Tonotopic organization in the medial geniculate body of the cat. *Brain Res.* 26, 402–405. doi: 10.1016/S0006-8993(71)80015-X

Anderson, L. A., and Linden, J. F. (2011). Physiological differences between histologically defined subdivisions in the mouse auditory thalamus. *Hear. Res.* 274, 48–60. doi: 10.1016/j.heares.2010.12.016

Aschoff, A., and Ostwald, J. (1987). Different origins of cochlear efferents in some bat species, rats, and guinea pigs. *J. Comp. Neurol.* 264, 56–72. doi: 10.1002/cne.902640106

Banks, M., and Smith, P. (1992). Intracellular recordings from neurobiotin-labeled cells in brain slices of the rat medial nucleus of the trapezoid body. *J. Neurosci.* 12, 2819–2837. doi: 10.1523/JNEUROSCI.12-07-02819.1992

Barker, A. J., Koch Lewin, G. R., and Pyott, S. J. (2021). Hearing and vocalizations in the naked mole-rat. *Adv. Exp. Med. Biol.* 1319, 157–195. doi: 10.1007/978-3-030-65943-1

Beyerl, B. D. (1978). Afferent projections to the central nucleus of the inferior colliculus in the rat. *Brain Res.* 145, 209–223. doi: 10.1016/0006-8993(78)90858-2

Bishop, A. L., and Henson, O. W. (1987). The efferent cochlear projections of the superior olivary complex in the mustached bat. *Hear. Res.* 31, 175–182. doi: 10.1016/0378-5955(87)90124-9

Boudreau, J. C., and Tsuchitani, C. (1970). Cat superior olive S-segment cell discharge to tonal stimulation. *Contrib. Sens. Physiol.* 4, 143–213. doi: 10.1016/B978-0-12-151804-2.50011-5

Bourk, T. R., Mielcarz, J. P., and Norris, B. E. (1981). Tonotopic organization of the anteroventral cochlear nucleus of the cat. *Hear. Res.* 4, 215–241. doi: 10.1016/0378-5955(81)90008-3

Brain Map - brain-map.org (2021). *Accelerating progress toward understanding the brain*. Retrieved 1 December 2021, from https://portal.brain-map.org.

Brown, M. C. (1987). Morphology of labeled afferent fibers in the guinea pig cochlea. *J. Comp. Neurol.* 260, 591–604. doi: 10.1002/cne.902600411

Brown, M. C. (1993). Fiber pathways and branching patterns of biocytin-labeled olivocochlear neurons in the mouse brainstem. *J. Comp. Neurol.* 337, 600–613. doi: 10.1002/cne.903370406

Brown, M. C. (2011). "Anatomy of olivocochlear neurons," in *Auditory and vestibular efferents*, eds D. K. Ryugo, R. R. Fay, and A. N. Popper (Berlin: Springer), 17–33. doi: 10.1007/978-1-4419-7070-1_2

Brown, M. C., and Levine, J. L. (2008). Dendrites of medial olivocochlear neurons in mouse. *Neuroscience* 154, 147–159. doi: 10.1016/j.neuroscience.2007.12.045

Brown, M. C., Liberman, M. C., Benson, T. E., and Ryugo, D. K. (1988). Brainstem branches from olivocochlear axons in cats and rodents. *J. Comp. Neurol.* 278, 591–603. doi: 10.1002/cne.902780410

Browner, R. H., and Webster, D. B. (1975). Projections of the trapezoid body and the superior olivary complex of the kangaroo rat (*Dipodomys merriami*). *Brain Behav. Evol.* 11, 338–354. doi: 10.1159/000123644

Brugge, J. F. (1988). "Stimulus coding in the developing auditory system," in *Auditory function: Neurobiological Bases of hearing*, eds G. M. Edelman, W. E. Gall, and W. M. Cowan (Hoboken, NJ: Wiley), 113–136.

Brunso-Bechtold, J. K., Linville, M. C., and Henkel, C. K. (1994). Terminal types on ipsilaterally and contralaterally projecting lateral superior olive cells. *Hear. Res.* 77, 99–104. doi: 10.1016/0378-5955(94)90257-7

Brunso-Bechtold, J. K., Thompson, G. C., and Masterton, R. B. (1981). HRP study of the organization of auditory afferents ascending to central nucleus of inferior colliculus in cat. *J. Comp. Neurol.* 197, 705–722. doi: 10.1002/cne.901970410

Calford, M. B., Webster, W. R., and Semple, M. M. (1983). Measurement of frequency selectivity of single neurons in the central auditory pathway. *Hear. Res.* 11, 395–401. doi: 10.1016/0378-5955(83)90070-9

Campbell, J. P., and Henson, M. M. (1988). Olivocochlear neurons in the brainstem of the mouse. *Hear. Res.* 35, 271–274. doi: 10.1016/0378-5955(88)90124-4

Cant, N. B. (1984). The fine structure of the lateral superior olivary nucleus of the cat. *J. Comp. Neurol.* 227, 63–77. doi: 10.1002/cne.902270108

Cant, N. B., and Casseday, J. H. (1986). Projections from the anteroventral cochlear nucleus to the lateral and medial superior olivary nuclei. *J. Comp. Neurol.* 247, 457–476. doi: 10.1002/cne.902470406

Doucet, J. R., and Ryugo, D. K. (2003). Axonal pathways to the lateral superior olive labeled with biotinylated dextran amine injections in the dorsal cochlear nucleus of rats. *J. Comp. Neurol.* 461, 452–465. doi: 10.1002/cne.10722

Ehret, G., and Riecke, S. (2001). Mice and humans perceive multiharmonic communication sounds in the same way. *Proc. Natl. Acad. Sci.* 99, 479–482. doi: 10.1073/pnas.012361999

Erickson, R. P., Hall, W. C., Jane, J. A., Snyder, M., and Diamond, I. T. (1967). Organization of the posterior dorsal thalamus of the hedgehog. *J. Comp. Neurol.* 131, 103–130. doi: 10.1002/cne.901310204

Eybalin, M. (1993). Neurotransmitters and neuromodulators of the mammalian cochlea. *Physiol. Rev.* 73, 309–373. doi: 10.1152/physrev.1993.73.2.309

Finlayson, P. G., and Caspary, D. M. (1991). Low-frequency neurons in the lateral superior olive exhibit phase-sensitive binaural inhibition. *J. Neurophysiol.* 65, 598–605. doi: 10.1152/jn.1991.65.3.598

Fisher, M., and Llewellyn, G. (1978). The Mongolian gerbil: Natural history, care, and maintenance. *Am. Biol. Teach.* 40, 557–560. doi: 10.2307/4446413

FitzPatrick, K. A. (1975). Cellular architecture and topographic organization of the inferior colliculus of the squirrel monkey. *J. Comp. Neurol.* 164, 185–207. doi: 10.1002/cne.901640204

Franken, T. P., Joris, P. X., and Smith, P. H. (2018). Principal cells of the brainstem's interaural sound level detector are temporal differentiators rather than integrators. *eLife* 7:e33854. doi: 10.7554/eLife.33854

Fredrich, M., Reisch, A., and Illing, R.-B. (2009). Neuronal subtype identity in the rat auditory brainstem as defined by molecular profile and axonal projection. *Exp. Brain Res.* 195, 241–260. doi: 10.1007/s00221-009-1776-7

Friauf, E., and Ostwald, J. (1988). Divergent projections of physiologically characterized rat ventral cochlear nucleus neurons as shown by intra-axonal injection of horseradish peroxidase. *Exp. Brain Res.* 73, 263–284. doi: 10.1007/BF00248219

Friauf, E., Krächan, E. G., and Müller, N. I. C. (2019). "Lateral superior olive," in *The oxford handbook of the auditory brainstem*, ed. K. Kandler (New York, NY: Oxford University Press), 328–394. doi: 10.1093/oxfordhb/9780190849061.013.10

Glendenning, K. K., and Masterton, R. B. (1983). Acoustic chiasm: Efferent projections of the lateral superior olive. *J. Neurosci.* 3, 1521–1537. doi: 10.1523/JNEUROSCI.03-08-01521.1983

Glendenning, K. K., Baker, B. N., Hutson, K. A., and Masterton, R. B. (1992). Acoustic chiasm V: Inhibition and excitation in the ipsilateral and contralateral projections of LSO. *J. Comp. Neurol.* 319, 100–122. doi: 10.1002/cne.903190110

Glendenning, K. K., Brusno-Bechtold, J. K., Thompson, G. C., and Masterton, R. B. (1981). Ascending auditory afferents to the nuclei of the lateral leminiscus. *J. Comp. Neurol.* 197, 673–703. doi: 10.1002/cne.901970409

Glendenning, K. K., Hutson, K. A., Nudo, R. J., and Masterton, R. B. (1985). Acoustic chiasm II: Anatomical basis of binaurality in lateral superior olive of cat. *J. Comp. Neurol.* 232, 261–285. doi: 10.1002/cne.902320210

Gómez-Álvarez, M., and Saldaña, E. (2015). Different tonotopic regions of the lateral superior olive receive a similar combination of afferent inputs. *J. Comp. Neurol.* 524, 2230–2250. doi: 10.1002/cne.23942

GraphPad Software, I. (2021). *GraphPad Prism 8*. La Jolla, CA: Graphpad.com.

Grothe, B. (1994). Interaction of excitation and inhibition in processing of pure tone and amplitude-modulated stimuli in the medial superior olive of the mustached bat. *J. Neurophysiol.* 71, 706–721. doi: 10.1152/jn.1994.71.2.706

Guinan, J. J., Norris, B. E., and Guinan, S. S. (1972). Single auditory units in the superior olivary complex: II: Locations of unit categories and tonotopic organization. *Int. J. Neurosci.* 4, 147–166. doi: 10.3109/00207457209164756

He, J. (2003). Slow oscillation in non-lemniscal auditory thalamus. *J. Neurosci.* 23, 8281–8290. doi: 10.1523/JNEUROSCI.23-23-08281.2003

He, Y., Kang, S. H., and Alvarez, L. (2021). Finding the Skeleton of 2D Shape and contours: Implementation of hamilton-jacobi skeleton. *Image Process. On Line* 11, 18–36. doi: 10.5201/ipol.2021.296

Heffner, R. S., and Heffner, H. E. (1993). Degenerate hearing and sound localization in naked mole rats (*Heterocephalus glaber*), with an overview of central auditory structures. *J. Comp. Neurol.* 331, 418–433. doi: 10.1002/cne.903310311

Helfert, R. H., and Schwartz, I. R. (1986). Morphological evidence for the existence of multiple neuronal classes in the cat lateral superior olivary nucleus. *J. Comp. Neurol.* 244, 533–549. doi: 10.1002/cne.902440409

Helfert, R. H., and Schwartz, I. R. (1987). Morphological features of five neuronal classes in the gerbil lateral superior olive. *Am. J. Anat.* 179, 55–69. doi: 10.1002/aja.1001790108

Helfert, R. H., Bonneau, J. M., Wenthold, R. J., and Altschuler, R. A. (1989). GABA and glycine immunoreactivity in the guinea pig superior olivary complex. *Brain Res.* 501, 269–286. doi: 10.1016/0006-8993(89)90644-6

Henkel, C. K., and Brunso-Bechtold, J. K. (1993). Laterality of superior olive projections to the inferior colliculus in adult and developing ferret. *J. Comp. Neurol.* 331, 458–468. doi: 10.1002/cne.903310403

Henkel, C. K., and Brunso-Bechtold, J. K. (1998). Calcium-binding proteins and GABA reveal spatial segregation of cell types within the developing lateral superior olivary nucleus of the ferret. *Microsc. Res. Tech.* 41, 234–245. doi: 10.1002/(SICI)1097-0029(19980501)41:3<234::AID-JEMT7>3.0.CO;2-T

Henkel, C. K., and Gabriele, M. L. (1999). Organization of the disynaptic pathway from the anteroventral cochlear nucleus to the lateral superior olivary nucleus in the ferret. *Anat. Embryol.* 199, 149–160. doi: 10.1007/s004290050216

Heth, G., Frankenberg, E., and Nevo, E. (1986). Adaptive optimal sound for vocal communication in tunnels of a subterranean mammal (*Spalax ehrenbergi*). *Experientia* 42, 1287–1289. doi: 10.1007/BF01946426

Hu, B. (2003). Functional organization of lemniscal and nonlemniscal auditory thalamus. *Exp. Brain Res.* 153, 543–549. doi: 10.1007/s00221-003-1611-5

Humason, G. L. (1979). *Animal tissue techniques*, 4th Edn. San Francisco, CA: W.H.Freeman and Company.

Imig, T. J., and Morel, A. (1985). Tonotopic organization in ventral nucleus of medial geniculate body in the cat. *J. Neurophysiol.* 53, 309–340. doi: 10.1152/jn.1985.53.1.309

Jenkins, S. A., and Simmons, D. D. (2006). GABAergic neurons in the lateral superior olive of the hamster are distinguished by differential expression of gad isoforms during development. *Brain Res.* 1111, 12–25. doi: 10.1016/j.brainres.2006.06.067

Joris, P. X. (1996). Envelope coding in the lateral superior olive. II. Characteristic delays and comparison with responses in the medial superior olive. *J. Neurophysiol.* 76, 2137–2156. doi: 10.1152/jn.1996.76.4.2137

Joris, P. X., and van der Heijden, M. (2019). Early binaural hearing: The comparison of temporal differences at the two ears. *Ann. Rev. Neurosci.* 42, 433–457. doi: 10.1146/annurev-neuro-080317-061925

Joris, P. X., and Yin, T. C. T. (1998). Envelope coding in the lateral superior olive. III. comparison with afferent pathways. *J. Neurophysiol.* 79, 253–269. doi: 10.1152/jn.1998.79.1.253

Kandler, K., Kullmann, P., Ene, F., and Kim, G. (2002). Excitatory action of an immature glycinergic/GABAergic sound localization pathway. *Physiol. Behav.* 77, 583–587. doi: 10.1016/S0031-9384(02)00905-8

Karnovsky, M. J., and Roots, L. (1964). A 'Direct-Coloring' thiocholine method for cholinesterases. *J. Histochem. Cytochem.* 12, 219–221. doi: 10.1177/12.3.219

Kelly, J. B., Liscum, A., van Adel, B., and Ito, M. (1998). Projections from the superior olive and lateral lemniscus to tonotopic regions of the rat's inferior colliculus. *Hear. Res.* 116, 43–54. doi: 10.1016/S0378-5955(97)00195-0

Kimura, A., Donishi, T., Sakoda, T., Hazama, M., and Tamai, Y. (2003). Auditory thalamic nuclei projections to the temporal cortex in the rat. *Neuroscience* 117, 1003–1016. doi: 10.1016/S0306-4522(02)00949-1

Komura, Y., Tamura, R., Uwano, T., Nishijo, H., and Ono, T. (2003). Transmodal coding for reward prediction in the audiovisual thalamus. *Int. Congr. Ser.* 1250, 383–396. doi: 10.1016/S0531-5131(03)01066-5

Konishi, S., Yuille, A. L., Coughlan, J. M., and Song Chun Zhu. (2003). Statistical edge detection: Learning and evaluating edge cues. *IEEE Trans. Pattern Anal. Mach. Intell.* 25, 57–74. doi: 10.1109/TPAMI.2003.1159946

Kulesza, R. J. (2007). Cytoarchitecture of the human superior olivary complex: Medial and lateral superior olive. *Hear. Res.* 225, 80–90. doi: 10.1016/j.heares.2006.12.006

Kulesza, R. J. (2008). Cytoarchitecture of the human superior olivary complex: Nuclei of the trapezoid body and posterior tier. *Hear. Res.* 241, 52–63. doi: 10.1016/j.heares.2008.04.010

Liberman, M. C., and Brown, M. C. (1986). Physiology and anatomy of single olivocochlear neurons in the cat. *Hear. Res.* 24, 17–36. doi: 10.1016/0378-5955(86)90003-1

Liu, M., Dai, J., Zhou, M., Liu, J., Ge, X., Wang, N., et al. (2022). Mini-review: The neural circuits of the non-lemniscal inferior colliculus. *Neurosci. Lett.* 776:136567. doi: 10.1016/j.neulet.2022.136567

Lu, E., Llano, D. A., and Sherman, S. M. (2009). Different distributions of calbindin and calretinin immunostaining across the medial and dorsal divisions of the mouse medial geniculate body. *Hear. Res.* 257, 16–23. doi: 10.1016/j.heares.2009.07.009

Lund, R. D., and Webster, K. E. (1967). Thalamic afferents from the spinal cord and trigeminal nuclei. An experimental anatomical study in the rat. *J. Comp. Neurol.* 130, 313–327. doi: 10.1002/cne.901300404

Maison, S. F., Adams, J. C., and Liberman, M. C. (2002). Olivocochlear innervation in the mouse: Immunocytochemical maps, crossed versus uncrossed contributions, and transmitter colocalization. *J. Comp. Neurol.* 455, 406–416. doi: 10.1002/cne.10490

Malmierca, M. S., Blackstad, T. W., and Osen, K. K. (2011). Computer-assisted 3-D reconstructions of Golgi-impregnated neurons in the cortical regions of the inferior colliculus of rat. *Hear. Res.* 274, 13–26. doi: 10.1016/j.heares.2010.06.011

Malmierca, M. S., Saint Marie, R. L., Merchan, M. A., and Oliver, D. L. (2005). Laminar inputs from dorsal cochlear nucleus and ventral cochlear nucleus to the central nucleus of the inferior colliculus: Two patterns of convergence. *Neuroscience* 136, 883–894. doi: 10.1016/j.neuroscience.2005.04.040

Mellott, J. G., Dhar, M., Mafi, A., Tokar, N., and Winters, B. D. (2021). Tonotopic distribution and inferior colliculus projection pattern of inhibitory and excitatory cell types in the lateral superior olive of Mongolian gerbils. *J. Comp. Neurol.* 530, 506–517. doi: 10.1002/cne.25226

Merzenich, M. M., and Reid, M. D. (1974). Representation of the cochlea within the inferior colliculus of the cat. *Brain Res.* 77, 397–415. doi: 10.1016/0006-8993(74)90630-1

Merzenich, M. M., Kitzes, L., and Aitkin, L. (1973). Anatomical and physiological evidence for auditory specialization in the mountain beaver (*aplodontia rufa*). *Brain Res.* 58, 331–344. doi: 10.1016/0006-8993(73)90005-X

Middlebrooks, J. C. (2015). Sound localization. *Handb. Clin. Neurol.* 129, 99–116. doi: 10.1016/B978-0-444-62630-1.00006-8

Middlebrooks, J. C., and Waters, M. F. (2020). Spatial mechanisms for segregation of competing sounds, and a breakdown in spatial hearing. *Front. Neurosci.* 14:571095. doi: 10.3389/fnins.2020.571095

Moore, D. R., Russell, F. A., and Cathcart, N. C. (1995). Lateral superior olive projections to the inferior colliculus in normal and unilaterally deafened ferrets. *J. Comp. Neurol.* 357, 204–216. doi: 10.1002/cne.903570203

Moore, J. K. (2000). Organization of the human superior olivary complex. *Microsc. Res. Tech.* 51, 403–412. doi: 10.1002/1097-0029(20001115)51:4<403::AID-JEMT8>3.0.CO;2-Q

Morest, D. K. (1964). The neuronal architecture of the medial geniculate body of the cat. *J. Anat.* 98, 611–630.

Mulders, W. H. A. M., and Robertson, D. (2004). Dopaminergic olivocochlear neurons originate in the high frequency region of the lateral superior olive of guinea pigs. *Hear. Res.* 187, 122–130. doi: 10.1016/S0378-5955(03)00308-3

Muniak, M. A., Ayeni, F. E., and Ryugo, D. K. (2018). Hidden hearing loss and endbulbs of Held: Evidence for central pathology before detection of ABR threshold increases. *Hear. Res.* 364, 104–117. doi: 10.1016/j.heares.2018.03.021

Muniak, M. A., Rivas, A., Montey, K. L., May, B. J., Francis, H. W., and Ryugo, D. K. (2013). 3D model of frequency representation in the cochlear nucleus of the CBA/J mouse. *J. Comp. Neurol.* 521, 1510–1532. doi: 10.1002/cne.23238

Nabekura, J., Katsurabayashi, S., Kakazu, Y., Shibata, S., Matsubara, A., Jinno, S., et al. (2003). Developmental switch from GABA to glycine release in single central synaptic terminals. *Nat. Neurosci.* 7, 17–23. doi: 10.1038/nn1170

Niu, X., Bogdanovic, N., and Canlon, B. (2004). The distribution and the modulation of tyrosine hydroxylase immunoreactivity in the lateral olivocochlear system of the guinea-pig. *Neuroscience* 125, 725–733. doi: 10.1016/j.neuroscience.2004.02.023

Nordeen, K. W., Killackey, H. P., and Kitzes, L. M. (1983). Ascending auditory projections to the inferior colliculus in the adult gerbil, Meriones unguiculatus. *J. Comp. Neurol.* 214, 131–143. doi: 10.1002/cne.902140203

Okanoya, K., Yosida, S., Barone, C. M., Applegate, D. T., Brittan-Powell, E. F., Dooling, R. J., et al. (2018). Auditory-vocal coupling in the naked mole-rat, a mammal with poor auditory thresholds. *J. Comp. Physiol. A* 204, 905–914. doi: 10.1007/s00359-018-1287-8

Oliver, D. L. (2000). Ascending efferent projections of the superior olivary complex. *Microsc. Res. Tech.* 51, 355–363. doi: 10.1002/1097-0029(20001115)51:4<355::AID-JEMT5>3.0.CO;2-J

Oliver, D. L., Beckius, G. E., Bishop, D. C., and Kuwada, S. (1997). Simultaneous anterograde labeling of axonal layers from lateral superior olive and dorsal cochlear nucleus in the inferior colliculus of cat. *J. Comp. Neurol.* 382, 215–229. doi: 10.1002/(SICI)1096-9861(19970602)382:2<215::AID-CNE6>3.0.CO;2-6

Ollo, C., and Schwartz, I. R. (1979). The superior olivary complex in C57BL/6 mice. *Am. J. Anat.* 155, 349–373. doi: 10.1002/aja.1001550306

Paxinos, G., and Franklin, B. J. (2008). *The mouse brain in stereotaxic coordinates*, 3rd Edn. Sydney, NSW: Elsevier.

Portfors, C. V., and Perkel, D. J. (2014). The role of ultrasonic vocalizations in mouse communication. *Curr. Opin. Neurobiol.* 28, 115–120. doi: 10.1016/j.conb.2014.07.002

Portfors, C. V., Mayko, Z. M., Jonson, K., Cha, G. F., and Roberts, P. D. (2011). Spatial organization of receptive fields in the auditory midbrain of awake mouse. *Neuroscience* 193, 429–439. doi: 10.1016/j.neuroscience.2011.07.025

Ramón y Cajal, S. (1909). *Histologie du Systeme Nerveux de L'Homme et des Vertebres, 1.* Paris: Maloine. doi: 10.5962/bhl.title.48637

Ramon-Moliner, E. (1962). An attempt at classifying nerve cells on the basis of their dendritic patterns. *J. Comp. Neurol.* 119, 211–227. doi: 10.1002/cne.901190207

Reiss, L. A. J., and Young, E. D. (2005). Spectral Edge sensitivity in neural circuits of the dorsal cochlear nucleus. *J. Neurosci.* 25, 3680–3691. doi: 10.1523/JNEUROSCI.4963-04.2005

Rietzel, H. J., and Friauf, E. (1998). Neuron types in the rat lateral superior olive and developmental changes in the complexity of their dendritic arbors. *J. Comp. Neurol.* 390, 20–40. doi: 10.1002/(SICI)1096-9861(19980105)390:1<20::AID-CNE3>3.0.CO;2-S

Rockel, A. J., and Jones, E. G. (1973). The neuronal organization of the inferior colliculus of the adult cat. I. The central nucleus. *J. Comp. Neurol.* 147, 11–59. doi: 10.1002/cne.901470103

Romand, R. (1983). Development in the frequency selectivity of auditory nerve fibers in the kitten. *Neurosci. Lett.* 35, 271–276. doi: 10.1016/0304-3940(83)90329-4

Romero, G. E., and Trussell, L. O. (2021). Distinct forms of synaptic plasticity during ascending vs descending control of medial olivocochlear efferent neurons. *eLife* 10:e66396. doi: 10.7554/eLife.66396

Rose, J. E., Greenwood, D. D., Goldberg, J. M., and Hind, J. E. (1963). Some discharge characteristics of single neurons in the inferior colliculus of the cat. I. Tonotopical organization, relation of spike-counts to tone intensity, and firing patterns of single elements. *J. Neurophysiol.* 26, 294–320. doi: 10.1152/jn.1963.26.2.294

Ross, L. S., Pollak, G. D., and Zook, J. M. (1988). Origin of ascending projections to an isofrequency region of the mustache bat's inferior colliculus. *J. Comp. Neurol.* 270, 488–505. doi: 10.1002/cne.902700403

Ryugo, D. K., and Fekete, D. M. (1982). Morphology of primary axosomatic endings in the anteroventral cochlear nucleus of the cat: A study of the endbulbs of Held. *J. Comp. Neurol.* 210, 239–257. doi: 10.1002/cne.902100304

Ryugo, D. K., and May, S. K. (1993). The projections of intracellularly labeled auditory nerve fibers to the dorsal cochlear nucleus of cats. *J. Comp. Neurol.* 329, 20–35. doi: 10.1002/cne.903290103

Safieddine, S., Prior, A. M., and Eyebalin, M. (1997). Choline acetyltransferase, glutamate decarboxylase, tyrosine hydroxylase, calcitonin gene-related peptide and opioid peptides coexist in lateral efferent neurons of rat and guinea-pig. *Eur. J. Neurosci.* 9, 356–367. doi: 10.1111/j.1460-9568.1997.tb01405.x

Saint Marie, R. L. S., Ostapoff, E.-M., Morest, D. K., and Wenthold, R. J. (1989). Glycine-immunoreactive projection of the cat lateral superior olive: Possible role in midbrain ear dominance. *J. Comp. Neurol.* 279, 382–396. doi: 10.1002/cne.902790305

Saint Marie, R. L., and Baker, R. A. (1990). Neurotransmitter-specific uptake and retrograde transport of [3H]glycine from the inferior colliculus by ipsilateral projections of the superior olivary complex and nuclei of the lateral lemniscus. *Brain Res.* 524, 244–253. doi: 10.1016/0006-8993(90)90698-B

Sánchez-González, M. A., Warr, W. B., and López, D. E. (2003). Anatomy of olivocochlear neurons in the hamster studied with FluoroGold. *Hear. Res.* 185, 65–76. doi: 10.1016/S0378-5955(03)00213-2

Sanes, D. H., Goldstein, N. A., Ostad, M., and Hillman, D. E. (1990). Dendritic morphology of central auditory neurons correlates with their tonotopic position. *J. Comp. Neurol.* 294, 443–454. doi: 10.1002/cne.902940312

Sanes, D., and Rubel, E. (1988). The ontogeny of inhibition and excitation in the gerbil lateral superior olive. *J. Neurosci.* 8, 682–700. doi: 10.1523/JNEUROSCI.08-02-00682.1988

Scheibel, M. E., and Scheibel, A. B. (1966). The organization of the nucleus reticularis thalami: A Golgi study. *Brain Res.* 1, 43–62. doi: 10.1016/0006-8993(66)90104-1

Scheibel, M. E., and Scheibel, A. B. (1974). Neuropil organization in the superior olive of the cat. *Exp. Neurol.* 43, 339–348. doi: 10.1016/0014-4886(74)90175-7

Schindelin, J., Arganda-Carreras, I., Frise, E., Kaynig, V., Longair, M., Pietzsch, T., et al. (2012). Fiji: An open-source platform for biological-image analysis. *Nat. Methods* 9, 676–682. doi: 10.1038/nmeth.2019

Schofield, B. R., and Cant, N. B. (1992). Organization of the superior olivary complex in the guinea pig: II. Patterns of projection from the periolivary nuclei to the inferior colliculus. *J. Comp. Neurol.* 317, 438–455. doi: 10.1002/cne.903170409

Schweizer, H. (1981). The connections of the inferior colliculus and the organization of the brainstem auditory system in the greater horseshoe bat (*Rhinolophus ferrumequinum*). *J. Comp. Neurol.* 201, 25–49. doi: 10.1002/cne.902010104

Sommer, I., Lingenhöhl, K., and Friauf, E. (1993). Principal cells of the rat medial nucleus of the trapezoid body: An intracellular in vivo study of their physiology and morphology. *Exp. Brain Res.* 95, 223–239. doi: 10.1007/BF00229781

Spirou, G. A., May, B. J., Wright, D. D., and Ryugo, D. K. (1993). Frequency organization of the dorsal cochlear nucleus in cats. *J. Comp. Neurol.* 329, 36–52. doi: 10.1002/cne.903290104

Stiebler, I., and Ehret, G. (1985). Inferior colliculus of the house mouse. I. A quantitative study of tonotopic organization, frequency representation, and tone-threshold distribution. *J. Comp. Neurol.* 238, 65–76. doi: 10.1002/cne.902380106

Suthakar, K. (2016). *Changes in the descending auditory system in hearing loss: Focus on auditory efferents.* PhD thesis. Sydney: University of New South Wales.

Taberner, A. M., and Liberman, M. C. (2005). Response properties of single auditory nerve fibers in the mouse. *J. Neurophysiol.* 93, 557–569. doi: 10.1152/jn.00574.2004

Thompson, G. C., and Thompson, A. M. (1986). Olivocochlear neurons in the squirrel monkey brainstem. *J. Comp. Neurol.* 254, 246–258. doi: 10.1002/cne.902540208

Tolbert, L. P., Morest, D. K., and Yurgelun-Todd, D. A. (1982). The neuronal architecture of the anteroventral cochlear nucleus of the cat in the region of the cochlear nerve root: Horseradish peroxidase labelling of identified cell types. *Neuroscience* 7, 3031–3052. doi: 10.1016/0306-4522(82)90228-7

Tollin, D. J. (2003). The lateral superior olive: A functional role in sound source localization. *Neuroscientist* 9, 127–143. doi: 10.1177/1073858403252228

Tollin, D. J., and Yin, T. C. T. (2002). The coding of spatial location by single units in the lateral superior olive of the cat. II. The determinants of spatial receptive fields in Azimuth. *J. Neurosci.* 22, 1468–1479. doi: 10.1523/JNEUROSCI.22-04-01468.2002

Tsuchitani, C. (1977). Functional organization of lateral cell groups of cat superior olivary complex. *J. Neurophysiol.* 40, 296–318. doi: 10.1152/jn.1977.40.2.296

Van Hooser, S. D. (2007). Similarity and diversity in visual cortex: Is there a unifying theory of cortical computation? *Neuroscientist* 13, 639–656. doi: 10.1177/1073858407306597

Vetter, D. E., Adams, J. C., and Mugnaini, E. (1991). Chemically distinct rat olivocochlear neurons. *Synapse* 7, 21–43. doi: 10.1002/syn.890070104

Vetter, D. E., and Mugnaini, E. (1992). Distribution and dendritic features of three groups of rat olivocochlear neurons. *Anat. Embryol.* 185, 1–16. doi: 10.1007/BF00213596

Warr, W. B. (1966). Fiber degeneration following lesions in the anterior ventral cochlear nucleus of the cat. *Exp. Neurol.* 14, 453–474. doi: 10.1016/0014-4886(66)90130-0

Warr, W. B. (1975). Olivocochlear and vestibular efferent neurons of the feline brain stem: Their location, morphology and number determined by retrograde axonal transport and acetylcholinesterase histochemistry. *J. Comp. Neurol.* 161, 159–181. doi: 10.1002/cne.901610203

Warr, W. B., and Guinan, J. J. (1979). Efferent innervation of the organ of corti: Two separate systems. *Brain Res.* 173, 152–155. doi: 10.1016/0006-8993(79)91104-1

Warr, W. B., Boche, J. B., and Neely, S. T. (1997). Efferent innervation of the inner hair cell region: Origins and terminations of two lateral olivocochlear systems. *Hear. Res.* 108, 89–111. doi: 10.1016/S0378-5955(97)00044-0

Wepsic, J. G. (1966). Multimodal sensory activation of cells in the magnocellular medial geniculate nucleus. *Exp. Neurol.* 15, 299–318. doi: 10.1016/0014-4886(66)90053-7

White, J. S., and Warr, B. W. (1983). The dual origins of the olivocochlear bundle in the albino rat. *J. Comp. Neurol.* 219, 203–214. doi: 10.1002/cne.902190206

Willard, F. H., and Martin, G. F. (1984). Collateral innervation of the inferior colliculus in the North American opossum: A study using fluorescent markers in a double-labeling paradigm. *Brain Res.* 303, 171–182. doi: 10.1016/0006-8993(84)90225-7

Wu, J. S., Yi, E., Manca, M., Javaid, H., Lauer, A. M., and Glowatzki, E. (2020). Sound exposure dynamically induces dopamine synthesis in cholinergic LOC efferents for feedback to auditory nerve fibers. *eLife* 9:e52419. doi: 10.7554/eLife.52419

Yao, W., and Godfrey, D. A. (1995). Immunohistochemistry of muscarinic acetylcholine receptors in rat cochlear nucleus. *Hear. Res.* 89, 76–85. doi: 10.1016/0378-5955(95)00123-7

Yin, T. C. T., Smith, P. H., and Joris, P. X. (2019). Neural mechanisms of binaural processing in the auditory brainstem. *Comp. Physiol.* 9, 1503–1575. doi: 10.1002/cphy.c180036

Young, E. D., Spirou, G. A., John, J. R., and Herbert, F. V. (1992). Neural organization and responses to complex stimuli in the dorsal cochlear nucleus. Philosophical transactions of the royal society of London. *Ser. B Biol. Sci.* 336, 407–413. doi: 10.1098/rstb.1992.0076

Zheng, Q. Y., Johnson, K. R., and Erway, L. C. (1999). Assessment of hearing in 80 inbred strains of mice by ABR threshold analyses. *Hear. Res.* 130, 94–107. doi: 10.1016/S0378-5955(99)00003-9